Reparative macrophages regulate fibrosis in the infarcted myocardium by attenuating apoptosis and senescence of fibroblasts

Manabu Shiraishi[1,2], Atsushi Yamaguchi[1] and Ken Suzuki[2]

[1]Department of Cardiovascular Surgery, Saitama Medical Center, Jichi Medical University, Saitama, Japan.

[2]William Harvey Research Institute, Barts and The London School of Medicine and Dentistry, Queen Mary University of London, London, United Kingdom.

Address correspondence to:

Manabu Shiraishi, Department of Cardiovascular Surgery, Saitama Medical Center, Jichi Medical University, Saitama, Japan.

Phone: +81-48-647-2111; e-mail: manabu@omiya.jichi.ac.jp

Conflict of interest statement:

The authors have declared that no conflict of interest exists.

This PDF file includes:

Main text

Figures 1 to 9

Abstract

Appropriate fibrotic tissue formation after myocardial infarction (MI) is crucial for maintaining the structure of the heart. Reparative (or M2-like) macrophages play a vital role in fibrosis by activating cardiac fibroblasts after MI. This study aimed to investigate the molecular and cellular mechanisms by which post-MI fibrosis is formed by focusing on the role of the M2-like macrophage subset, and to examine how formation of fibrosis can be controlled. We found that cardiac fibroblasts in the infarcted mouse heart showed apoptosis and senescence, both of which are associated with the fibrotic process. Moreover, we discovered that part of the molecular mechanism underlying fibrotic tissue formation in the infarcted myocardium was attenuation of apoptosis and senescence of fibroblasts by neuregulin 1 (Nrg1)/epidermal growth factor receptor signaling. We analyzed $CD206^{+}F4/80^{+}CD11b^{+}$ M2-like macrophages in intact and infarcted hearts and identified increased Nrg1 expression in M2-like macrophages in the infarcted heart. *In vitro* and *in vivo* studies showed that selective Nrg1 receptor inhibition exacerbated senescence of cardiac fibroblasts, which resulted in excessive progression of fibrosis. These results highlight previously unidentified anti-apoptotic and anti-senescence effects of Nrg1 on cardiac fibroblasts after MI and represent the potential basis for a viable therapeutic strategy for MI.

42 **Introduction**

43

44 Myocardial infarction (MI) is one of the leading causes of mortality and disability. Even survivors of
45 acute MI frequently develop heart failure owing to adverse ventricular remodeling (1, 2). Because the
46 human heart has an insufficient regenerative ability, connective tissue formation is essential for
47 maintaining integrity and rigidity of the heart. However, the mechanism by which cardiac fibrosis is
48 regulated post-MI is not fully understood.

49 MI causes permanent loss of hundreds of millions of cardiomyocytes (3). Studies have also shown
50 that even non-cardiomyocytes, including fibroblasts, disappear by apoptosis in large quantities in the
51 infarcted area, and that senescence-associated defects occur in cardiac repair after MI (4, 5).
52 Apoptosis plays an important role in the disappearance of infiltrated immune cells and interstitial
53 cardiac cells after MI (5). Determining the effects of apoptosis and senescence on cell function during
54 the tissue repair process after MI is important. Cellular senescence and apoptosis are processes of
55 growth arrest in response to cellular stress and damage, and they limit proliferation of mammalian
56 cells (6, 7). Senescent cells show a complex phenotype, characterized by cell cycle arrest mediated by
57 the p16 and p53/p21 pathways, and a unique secretory phenotype, known as the
58 senescence-associated secretory phenotype (SASP) (8). Cell cycle arrest plays a central role in the
59 senescent phenotype of adult cardiomyocytes, and induction of cell cycle reentry of adult
60 cardiomyocytes promotes cardiac repair post-MI (9). Furthermore, anti-apoptotic substances and Fas
61 receptor competitive inhibitors are able to inhibit cardiomyocyte apoptosis, resulting in a decrease in
62 the infarct size and an improvement in cardiac function after MI (10).

63 Previous studies have shown that even non-cardiomyocytes, including fibroblasts, undergo
64 apoptosis in the infarcted area (4, 5). Therefore, cellular senescence and/or apoptosis in cardiac
65 fibroblasts, not limited to cardiomyocytes, is likely to be involved in the tissue repair process after MI.
66 To some extent, senescence of fibroblasts restricts fibrosis in itself, but the long-term presence of this
67 condition is deleterious in the tissue repair process (11). Proper fibrosis after MI is crucial for
68 maintaining the structure of the heart, but excessive fibrosis eventually leads to heart failure.
69 Therefore, adjusting the balance between a pro-fibrotic versus an anti-fibrotic environment is

important for a successful regenerative outcome. To understand the tissue repair process of fibrosis, clarifying intercellular communication between senescent and apoptotic fibroblasts and surrounding cells is necessary.

Recent studies have shown that macrophages are essential factors in regeneration of the neonatal mouse heart (12). We have previously shown that reparative (or M2-like) macrophages play a pivotal role in fibrotic tissue formation post-MI through promotion of proliferation and activation of cardiac fibroblasts (13). However, the molecular mechanism used by M2-like macrophages in the anti-senescence and anti-fibrotic environment after MI remains unknown. We hypothesize that M2-like macrophages play a vital role in attenuating apoptosis and senescence, which cause excessive fibrosis, of cardiac fibroblasts.

Neuregulin 1 (Nrg1) is one of the neuregulin genes (*Nrg1–Nrg4*) that belong to the epidermal growth factor family (14, 15), and it plays essential roles in protection and proliferation of cardiomyocytes in response to injury (16-20). Although the association between Nrg1 and protection of cardiomyocytes has been studied for several decades (16-20), the role of Nrg1 in protecting cardiac fibroblasts and in post-MI regeneration has not yet been established. This study aimed to investigate the molecular and cellular mechanism by which post-MI fibrosis is formed with a focus on the role of the M2-like macrophage subset, and to examine how formation of fibrosis can be controlled. The findings of this study are expected to help clarify the pathophysiology of fibrosis after MI and to form the basis for development of new therapeutic methods focused on senescence and apoptosis of cardiac fibroblasts.

Results

Cardiac fibroblasts undergo apoptosis and senescence after MI

First, we investigated the occurrence of cellular senescence and apoptosis in the process of post-MI fibrosis in a mouse model of MI based on coronary artery ligation. In this model, obvious fibrotic tissue formation and increased myocardial expression of fibrosis-associated genes (i.e., alpha-smooth muscle actin [*αSMA*], *Col1a1,* and *Col3a1*) were observed in the infarct area as early as day 7 post-MI

98 (Supplemental Figure 1A, B). This change was associated with an increase in Thy1$^+$ fibroblasts and
99 Thy1$^+$αSMA$^+$ myofibroblasts in the infarct area (Supplemental Figure 1C, D) with a peak at day 7
100 post-MI. Approximately, 40% and 15% of Thy1$^+$ fibroblasts were positive for cleaved caspase-3 in
101 the infarct area on days 7 and 28 after MI, respectively, which suggested robust occurrence of
102 apoptosis in cardiac fibroblasts. Cleaved caspase-3-positive cardiac fibroblasts were rarely found in
103 the non-infarcted remote area (Figure 1A). Simultaneously, senescence-associated beta galactosidase
104 (SA-β-Gal)-positive cells were found in the same infarct area. These cells showed a spindle shape
105 with many cytoplasmic processes, which suggested that they were fibroblasts (Figure 1B).
106 Additionally, myocardial expression of senescence-associated genes (i.e., *SA-β-Gal, p16, p53,* and
107 *p21*) (1, 6, 7, 21, 22) was upregulated in the infarct area compared with the non-infarcted remote area
108 (Figure 1C). Increased apoptosis and senescence in fibroblasts (and other types of cardiac cells)
109 exacerbated myocardial inflammation post-MI (Supplemental Figure 1E). Taken together, these
110 results suggest that apoptosis and senescence occur in cardiac fibroblasts during the process of fibrotic
111 tissue formation in the post-MI heart.
112
113 ***Nrg1 is upregulated in the infarcted myocardium, while cardiac fibroblasts express Nrg1 receptors***
114 Quantitative reverse transcription-polymerase chain reaction (qRT-PCR) data showed that *Nrg1* was
115 upregulated in the infarct area of the mouse heart with a peak on day 7 post-MI (Figure 2A).
116 Immunohistochemistry (IHC) showed that most of the Thy1$^+$ cardiac fibroblasts that had accumulated
117 in infarcted and remote areas expressed epidermal growth factor receptor (ErbB) 2 and ErbB4, which
118 are co-receptors of Nrg1 (20, 23, 24). However, fibroblasts in the intact heart (no MI) did not express
119 these receptors (Figure 2B). These results suggest that Nrg1 is involved in changes in cardiac
120 fibroblasts after MI.
121
122 ***M2-like macrophages accumulate in the infarct area and express Nrg1***
123 M2-like macrophages play an important role in fibrotic tissue formation post-MI (13). IHC showed
124 that CD206$^+$ M2-like macrophages had accumulated in the infarct area with a peak at day 7 post-MI
125 (Figure 3A). Interestingly, this change in M2-like macrophages post-MI corresponded to a change in

126 occurrence of cardiac fibroblasts post-MI (Supplemental Figure 1C). We found that $CD206^+$ cells
127 were also positive for F4/80 in the intact and MI heart (Figure 3B). Microarray analysis showed that
128 $CD206^+F4/80^+CD11b^+$ M2-like macrophages that were collected from hearts on day 7 after MI had a
129 different molecular signature than that in those from intact hearts (Supplemental Figure 2A). A range
130 of anti-inflammatory and reparative genes were upregulated in M2-like macrophages from MI hearts
131 compared with intact hearts (Supplemental Figure 2B; full data are available in the Gene Expression
132 Omnibus [GEO] database; GSE69879). Importantly, gene ontology analysis showed that M2-like
133 macrophages that were collected from hearts on day 7 after MI were associated with regulation of
134 apoptosis and cell death (Supplemental Figure 2C). In particular, increased *Nrg1* expression levels in
135 $CD206^+F4/80^+CD11b^+$ cardiac M2-like macrophages were observed after MI (Figure 3C), which was
136 further confirmed by qRT-PCR and IHC (Figure 3D, E). These data suggest that cardiac M2-like
137 macrophages may be one of the major sources of upregulation of Nrg1 post-MI.
138
139 ***Bone marrow-derived macrophages attenuate H_2O_2-induced apoptosis and senescence of cardiac***
140 ***fibroblasts via Nrg1 secretion***
141 We then investigated the role of macrophages in regulating senescence and apoptosis in *in vitro*
142 co-culture of cardiac fibroblasts with bone marrow-derived macrophages (BMDMs) using a Boyden
143 Chamber system (13, 25) (Supplemental Figure 3A). H_2O_2 was used to induce apoptosis and
144 senescence in fibroblasts (Supplemental Figure 3B, C). BMDMs cultured in the presence of H_2O_2
145 showed an M2-like macrophage phenotype (Supplemental Figure 4A, B). Expression of *Nrg1* in
146 BMDMs and *ErbB2* and *ErbB4* in isolated cardiac fibroblasts was observed (Supplemental Figure
147 5A–C). This gene expression was upregulated in response to H_2O_2. Phase-contrast microscopy
148 showed that fibroblasts treated with H_2O_2 had an enlarged, flattened, senescent morphology, which
149 became a spindle-shaped healthy form after co-culture with BMDMs. Senescent fibroblasts treated
150 with anti-ErbB4 antibody (ErbB Ab), which is a competitive inhibitor of Nrg1, displayed the same
151 gross morphology as senescent fibroblasts treated with H_2O_2. Recombinant Nrg1 similarly changed
152 the gross morphology of senescent fibroblasts treated with H_2O_2 to a spindle-shaped healthy form
153 again (Figure 4A). SA-β-Gal staining showed that approximately 20% of fibroblasts treated with

154 H_2O_2 became positive for SA-β-Gal. This change was significantly attenuated by co-culture with
155 BMDMs, while addition of ErbB Ab eliminated this anti-senescence effect of BMDMs. Furthermore,
156 administration of recombinant Nrg1 suppressed H_2O_2-induced senescence of fibroblasts (Figure 4B).
157 The ratio of cleaved caspase 3^+ apoptotic cells in cardiac fibroblasts was also significantly increased
158 with H_2O_2 stimulation (Figure 4C). Co-culture with BMDMs markedly attenuated this apoptotic
159 change in fibroblasts. This anti-apoptotic effect of BMDMs was attenuated by addition of ErbB Ab,
160 while administration of recombinant Nrg1 suppressed H_2O_2-induced apoptosis of fibroblasts.
161 Immunolabeling for Ki67 and a scratch assay showed that proliferation and migratory properties in
162 cardiac fibroblasts were significantly attenuated with H_2O_2 stimulation (Figure 4D and Supplemental
163 Figure 6). Co-culture with BMDMs markedly improved these cellular activities in fibroblasts. These
164 effects of BMDMs were attenuated by addition of ErbB Ab, while administration of recombinant
165 Nrg1 suppressed H_2O_2-induced functional deterioration of fibroblasts. H_2O_2 stimulation reduced
166 proliferation and migration of cardiac fibroblasts, which were rescued by co-culture with BMDMs.
167 This effect of BMDMs was eliminated by addition of ErbB Ab. Recombinant Nrg1 administration
168 showed a strong ability to increase proliferation of fibroblasts. These results collectively suggest that
169 M2-like macrophages reduce apoptosis and senescence of fibroblasts through secretion of Nrg1.
170
171 ***BMDMs promote activation of fibroblasts and collagen synthesis***
172 Immunocytological staining showed that, although independent H_2O_2 treatment did not affect
173 transformation of cardiac fibroblasts into αSMA^+ myofibroblasts, co-culture with BMDMs and H_2O_2
174 stimulation induced activation of fibroblasts. Furthermore, addition of ErbB Ab enhanced this
175 BMDM-induced activation of fibroblasts. Moreover, addition of recombinant Nrg1 did not affect
176 transformation of cardiac fibroblasts (Figure 5A). Changes in synthesis of types I and III collagen in
177 fibroblasts in response to H_2O_2, BMDMs, and Nrg1 were associated with that of αSMA expression
178 (Figure 5B, C). These results suggest that BMDMs, which have an M2-like phenotype (Supplemental
179 Figure 4A, B), induce activation of fibroblasts to myofibroblasts, and this activation is accelerated
180 with progression of senescence of fibroblasts. Osteopontin (*Spp1*) is a key mediator of M2-like
181 macrophage-induced cardiac fibroblast activation (13). *Spp1* expression was increased in BMDMs in

182 response to H_2O_2 (Supplemental Figure 7A). In contrast, other profibrotic factors, including *Tgfb1* and
183 *Pdgfa* (26, 27), were not upregulated in M2-like macrophages (Supplemental Figure 7B).
184
185 ***The phosphatidylinositol 3-kinase/protein kinase B signaling pathway is associated with***
186 ***BMDM-attenuated apoptosis and senescence of cardiac fibroblasts through Nrg1***

187 We then investigated a potential mechanism underlying attenuation of apoptosis of cardiac fibroblasts
188 and senescence by BMDMs and/or Nrg1. The phosphatidylinositol 3-kinase (PI3K)/protein kinase B
189 (Akt) signaling pathway is a downstream part of the ErbB pathway. Western blot analysis showed that
190 co-culture with BMDMs increased activation of PI3K/Akt in fibroblasts, while this was attenuated by
191 addition of ErbB Ab. Recombinant Nrg1 administration also activated the PI3K/Akt pathway in
192 fibroblasts (Figure 6A). To determine the possible relationship between senescence-associated
193 p16/p53/p21 and the Nrg1/ErbB/PI3K/Akt signaling pathways, we examined mRNA expression
194 levels of senescence-associated genes (*p53, p21*, *p16, and SA-β-Gal)* (Figure 6B), cell
195 cycle-associated genes (cyclin-dependent kinase 4 [*Cdk4*], cyclin-dependent kinase 6 [*Cdk6*],
196 cyclin-dependent kinase 2 [*Cdk2*], and *Ki-67*) (Figure 6C), a p53 suppressor gene (murine double
197 minute 2 [*MDM2*]) (Figure 6D), a cell survival-associated gene (mechanistic target of rapamycin
198 [*mTOR*]) (Figure 6E), and an SASP-associated gene (interleukin-6 [*IL-6*]) (Figure 6F). Expression of
199 senescence-associated genes (*p16* and *p21*) and an SASP-associated gene (*IL-6*) was significantly
200 higher, and expression of cell cycle-associated genes (*Cdk4, Cdk6, Cdk2,* and *Ki-67*) and a cell
201 survival-associated gene (*mTOR*) was markedly lower in fibroblasts treated with H_2O_2 compared with
202 controls. Importantly, these changes in gene expression, including progression of senescence and
203 inflammation, and suppression of the cell cycle, recovered to those of controls by co-culture with
204 BMDMs. Addition of ErbB Ab resulted in gene expression similar to that with H_2O_2 treatment.
205 Moreover, expression of senescence-associated genes (*p53*, *p16,* and *p21)* was significantly
206 suppressed, and expression of cell cycle-associated genes (*Cdk4, Cdk6, Cdk2,* and *Ki-67*) was
207 enhanced by recombinant Nrg1 in fibroblasts treated with H_2O_2. For other related genes, BMDMs

208 enhanced expression of the p53 suppressor gene *MDM2*. These results suggest that the Nrg1/ErbB
209 system operates downstream of PI3K/Akt signaling activation and exerts a suppressive effect on cell
210 cycle arrest, senescence, and apoptosis. At the same time, this signaling activity is likely to increase
211 cellular proliferation and survival (Figure 6G).
212

213 ***In vivo inhibition of Nrg1 signaling exacerbates fibrosis***

214 We used trastuzumab to clarify the role of Nrg1 in suppressing senescence and apoptosis of cardiac
215 fibroblasts post-MI *in vivo*. Trastuzumab is an anti-human epidermal growth factor receptor type 2
216 (HER2) monoclonal antibody that binds to the extracellular juxtamembrane domain of HER2.
217 Trastuzumab is an effective treatment for HER2/neu^{+} tumors in animals and humans (28, 29). We
218 hypothesized that trastuzumab administration eliminates the anti-apoptotic and anti-senescence effects
219 of Nrg1, and therefore, trastuzumab increases the number of senescent cardiac fibroblasts. We also
220 hypothesized that, in the *in vitro* co-culture model, M2-like macrophages activate senescent
221 fibroblasts, resulting in escalation in fibrotic scar formation in the infarcted myocardium. We found
222 that intraperitoneal trastuzumab injections did not affect mRNA expression in the intact heart
223 (Supplemental Figure 8A–D).

224 Mice underwent surgery to induce MI and received intraperitoneal injections of either trastuzumab
225 or vehicle only (Supplemental Figure 9A). Trastuzumab did not affect post-MI mortality or body
226 weight (Supplemental Figure 9B, C). Gene expression profiles in the infarcted myocardium suggested
227 that apoptosis and senescence were augmented by trastuzumab administration in the infarct area
228 (Figure 7A–C). These changes in gene expression corresponded to an increase in apoptotic fibroblasts
229 and senescent cardiac cells in the infarct area (Figure 7D, E). Additionally, trastuzumab
230 administration increased fibrotic tissue formation in the infarct area (Figure 8A). In fact, the
231 occurrence of Thy-1^{+} fibroblasts in this area was increased (Figure 8B). The number of αSMA^{+}Thy1^{+}
232 myofibroblasts was also increased in association with upregulation of *αSMA*, *Col1a1,* and *Col3a*1 in
233 the infarcted myocardium (Figure 8B, C). Increased inflammation (Figure 9A) and increased
234 occurrence of M2-like macrophages in this area (Figure 9B) may explain these findings. Trastuzumab

235 administration might have increased apoptosis and senescence in fibroblasts (and other types of
236 cardiac cells), which exacerbated myocardial inflammation post-MI. This led to accumulation of
237 M2-like macrophages. Such augmented inflammatory signals or an increased number of M2-like
238 macrophages could accelerate proliferation of cardiac fibroblasts, while increased M2-like
239 macrophages could promote activation of fibroblasts to myofibroblasts. Subsequently, trastuzumab
240 administration might have exacerbated fibrotic tissue formation. This concept is supported by
241 additional findings in the non-infarcted remote area. Trastuzumab administration induced apoptosis-
242 and senescence-associated expression in the remote area (Supplemental Figure 10A–E) in which such
243 cell damage hardly occurred post-MI. This corresponded to increased inflammation (Supplemental
244 Figure 11A). These changes resulted in augmented accumulation of M2-like macrophages and cardiac
245 fibroblasts in the remote myocardium (Supplemental Figure 11B, 12A). Activation of fibroblasts to
246 myofibroblasts and fibrosis-associated gene expression were also prompted (Supplemental Figure
247 12A, B). Consequently, fibrosis occurred even in the remote area (Supplemental Figure 13A). These
248 results suggest that trastuzumab augments apoptosis and senescence of cardiac fibroblasts post-MI,
249 resulting in excessive fibrosis, even in the non-infarcted remote area.
250
251 **Discussion**
252
253 Despite the enormous clinical importance of cellular and molecular processes underlying the
254 formation of post-MI fibrosis, they are not well understood. In this study, we described the qualitative
255 changes in cardiac fibroblasts during formation of fibrosis post-MI. After MI, senescence and
256 apoptosis of cardiac fibroblasts occurred. However, Nrg1 suppressed senescence and apoptosis of
257 fibroblasts by activating the Nrg1/PI3K/Akt signaling pathway and indirectly decreased excessive
258 fibrosis. These results support our hypothesis that M2-like macrophages play a vital role in
259 suppressing senescence and apoptosis of fibroblasts and regulating collagen synthesis (Figure 9).
260 After induction of MI, senescence-associated gene expression (i.e., *SA-β-Gal*, *p53, p21,* and *p16*) was
261 significantly increased in the infarct area. Cardiac fibroblasts that were accumulated in the infarct area
262 expressed *SA-β-Gal* and cleaved caspase 3 at a certain ratio. One of the reparative genes, *Nrg1,* was

263 upregulated in the infarct area. Cardiac fibroblasts showed ErbB2/ErbB4, which are co-receptors of
264 Nrg1 (20, 23, 24), in the damaged myocardium. To precisely determine the role of cardiac M2-like
265 macrophages in the activity of apoptotic and senescent fibroblasts, we analyzed gene expression
266 profiling of these macrophages. Interestingly, we found more than four-fold upregulation of *Nrg1*
267 expression in M2-like macrophages in the post-MI heart compared with the normal heart. Our
268 findings were strengthened by an additional *in vitro* experiment in which H_2O_2-induced senescent
269 cardiac fibroblasts were co-cultured with BMDMs. Senescent cells attract macrophages in
270 pathological conditions (30). This model allowed us to determine the precise interaction between
271 M2-like macrophages and senescent cardiac fibroblasts. IHC showed that after the processes of
272 senescence and apoptosis of fibroblasts were improved by co-culture with BMDMs, addition of ErbB
273 Ab exacerbated them again. Simultaneously, western blot and qRT-PCR analysis showed that
274 PI3K/Akt signaling pathways were activated by co-culture with BMDMs and suppressed by adding
275 ErbB Ab. Furthermore, adding recombinant Nrg1 resulted in the same activation of PI3K/Akt
276 signaling pathways as co-culture with BMDMs. Additionally, co-culture with BMDMs promoted
277 H_2O_2-induced senescent fibroblasts to transform fibroblasts into αSMA^+ myofibroblasts, which
278 resulted in increased collagen synthesis. This activation and collagen synthesis were further
279 augmented by adding ErbB Ab. These results corresponded to *in vivo* observations with trastuzumab.
280 Intraperitoneal trastuzumab injections further increased senescence and secretion of SASP. This
281 exacerbation of inflammation induced by trastuzumab caused increased accumulation of M2-like
282 macrophages in the infarct area. IHC staining and qRT-PCR analysis showed that accumulation of
283 M2-like macrophages promoted proliferation and activation of fibroblasts, which resulted in
284 augmentation of fibrosis even in the non-infarcted remote area.
285 Nrg1 is a cytokine that belongs to a family of proteins structurally related to epidermal growth
286 factor and plays essential roles in protection and proliferation of cardiomyocytes in response to injury
287 (16-20). Nrg1 is synthesized in endothelial cells near cardiomyocytes (20). We observed that *Nrg1*
288 was expressed in M2-like macrophages and that it had a specific function for rescuing
289 post-MI-induced senescent and apoptotic cardiac fibroblasts. Cardiac fibroblasts showed
290 ErbB2/ErbB4 in the damaged myocardium on days 7 and 28 post-MI. Nrg1 binds to the ErbB4

291 receptor. After heterodimerization with phosphorylated ErbB2, signaling pathways that are activated
292 downstream of ErbB2/ErbB4 signals link to the Ras-mitogen-activated protein kinase pathway and
293 PI3K/Akt pathways (20). The hypertrophic response to Nrg1 is mainly Ras dependent, whereas the
294 anti-apoptotic and cell proliferation effects are likely to be Akt dependent (31-33). Therefore, Nrg1
295 could attenuate the senescence-associated genes *p53*, *p21*, and *p16* through the PI3K/Akt pathways. In
296 our study, we observed a transient increase in *p53*, *p21*, and *p16* expression in infarcted myocardium
297 and cultured fibroblasts. Zhu *et al*. reported that MI promoted accumulation of senescent cardiac
298 fibroblasts in the heart and *p53* expression (1). Increased p53 activity in response to diverse
299 pathological stresses, such as MI, induces apoptosis (34, 35). Stress-induced *p53* expression increases
300 *p21* expression in response to DNA damage and produces a reversible proliferative arrest that
301 provides time for DNA repair and facilitates survival of cells (36, 37). Previous studies have shown
302 that p21 binds to and inhibits CDK2-mediated inactivation of retinoblastoma, subsequently preventing
303 entry into the S phase of the cell cycle (7, 38). Furthermore, p21 is important for initiating senescence
304 in some settings, but its expression does not persist in senescent cells (39, 40). Simultaneously,
305 increased *p16* expression is found in infarct tissue. Irreversible proliferative arrest can be produced by
306 p16 inhibiting two cycle-dependent kinases, CDK4 and CDK6 (7, 41). Therefore, a change in
307 expression of these genes (i.e., *p53*, *p21*, and *p16*) in cardiac cells *in vivo* and cardiac fibroblasts *in*
308 *vitro* suggests that Nrg1 is a crucial factor controlling reversible and irreversible senescence of cardiac
309 cells after MI.

310 Previous reports have shown that trastuzumab efficiently stops or slows growth of $ErbB2^+$ cells
311 *in vitro* and inhibits the ability of cells to repair damaged DNA (28, 29). Our study showed that
312 trastuzumab injections further increased senescence and apoptosis in infarcted myocardium. As
313 inflammation worsens, M2-like macrophages from the bone marrow accumulate at the site of
314 damaged tissue (42). In our study, exacerbation of inflammation induced by trastuzumab caused
315 increased accumulation of M2-like macrophages and promoted proliferation and activation of
316 fibroblasts. Although we analyzed mRNA gene expression in tissue sections of the heart and not in
317 single cells, increased expression levels of senescence-associated genes were considered to reflect
318 senescence of fibroblasts to a certain extent. These results are consistent with our previous report,

319 which showed that osteopontin-mediated transformation of fibroblasts into myofibroblasts resulted in
320 progression of fibrosis (13). Interestingly, senescence and SASP-associated gene expression peaked
321 slightly later in the remote area than in the infarct area. One possible pathological mechanism of the
322 non-infarcted remote area is assumed to be indirect damage via SASP rather than direct cytotoxicity
323 due to ischemia. Senescent cells autonomously induce senescence-like gene expression in their
324 surrounding non-senescent cells through SASP (43). Increased SASP in the infarct area might not
325 simply reflect senescence and apoptosis in cells in the infarct area, but also changes in non-senescent
326 cells in the remote area. All of these data suggest that trastuzumab-induced exacerbation of fibrosis is
327 mainly mediated by progression of senescence and apoptosis in cardiac fibroblasts.
328 Our data provide new biological insights into the molecular mechanisms by which M2-like
329 macrophages regulate post-MI tissue repair by affecting senescence, apoptosis, and proliferation of
330 fibroblasts. This repair allows senescent cardiac fibroblasts to be maintained to a certain degree.
331 Although the process is not perfect, it allows them to survive. Incomplete rescue of fibroblasts from
332 senescence, mediated by M2-like macrophages, might lead to undesired fibrosis after diastolic
333 dysfunction. Although Nrg1 has been repeatedly reported to play important roles in injured
334 cardiomyocytes (16-20), its role in cardiac fibroblasts in this context has not been well studied. In our
335 study, the underlying molecular mechanisms of Nrg1 were investigated in experiments with
336 H_2O_2-induced senescent cardiac fibroblasts, and these showed activation of the p53/p21 and p16
337 pathways followed by cell cycle arrest. We present new *in vitro* evidence suggesting that M2-like
338 macrophages play a vital role for attenuating senescent and apoptotic fibroblasts through the
339 Nrg1/PI3K/Akt signaling pathways. This contributes to a variety of processes that are critical in
340 mediating many aspects of cellular function, including cell growth and survival (44). However,
341 further mechanistic studies are required to understand the signaling pathways downstream of these
342 factors and investigations in cell type-specific conditional *ErbB2/ErbB4*-knockout mice and to further
343 confirm the direct role of Nrg1 in cardiac fibroblasts. This knowledge could answer questions about
344 which cardiac cells are directly and indirectly affected, which cellular responses occur after MI, and
345 which signaling mechanisms are involved. Better understanding of the healing process of infarcts and
346 subsequent remodeling may result in new treatment options.

347 Although this study focused on Nrg1-induced anti-apoptosis and anti-senescence of cardiac
348 fibroblasts, M2-like macrophages are likely to mediate supplementary benefits in cardiac repair
349 post-MI. These benefits could include reduced inflammation, activation of fibroblasts, and
350 neovascular formation, as shown in our previous study (13). To develop potential therapies mediated
351 by M2-like macrophages, future studies will also need to determine how the gene that encodes Nrg1
352 is switched on by MI and to identify the other molecules that regulate apoptosis, senescence, and
353 proliferation of cardiac fibroblasts. There might be an alternative signal(s) to Nrg1 by which cardiac
354 M2-like macrophages induce proliferation of fibroblasts. This signal might be relatively negative
355 because we found that ErbB Ab totally depleted the ability of proliferation of fibroblasts from
356 BMDMs (Figure 4D).
357
358 In conclusion, our data provide evidence that Nrg1 critically regulates senescence and apoptosis of
359 cardiac fibroblasts in the infarcted adult murine heart and *in vitro* in a co-culture model. This process
360 could play a vital role in repair of the infarcted fragile ventricular wall and diastolic dysfunction due
361 to excessive fibrosis. Therefore, this tissue repair mechanism controls the degree of rigidity and
362 contraction of the infarcted heart, thus determining the prognosis post-MI. Targeted activation of
363 M2-like macrophages might enhance this endogenous repair mechanism in senescent cardiac
364 fibroblasts, suggesting that this approach could be a new therapeutic treatment of MI.
365
366 **Methods**
367
368 ***Animals.*** Eight- to 10-week-old mice were used in the experiments. C57BL/6 mice were purchased
369 from Tokyo Laboratory Animals Science Co., Ltd. The mice were maintained in a specific
370 pathogen-free room in our animal facility on a 12-hour light/dark cycle with free access to food and
371 water. The in vitro studies and in vivo procedures and assessments were performed in a blinded
372 manner.

373 ***In vivo treatments.*** Mice were treated with three i.p injections of 100 μg of Trastuzumab (Bio X Cell;
374 catalog BE0277) on the fourth, fifth, and sixth days after induction of myocardial infarction (MI).
375 Samples were collected on the seventh, 12th, and 28th days after induction of MI.
376 ***Preparation of bone marrow-derived macrophages (BMDMs).*** Mouse BMDMs were prepared from
377 the femurs and tibiae of 8-week-old wild type (WT) mice, as previously described (13). Bone marrow
378 mononuclear cells were collected by centrifugation on Ficoll-Paque (GE Healthcare) and were
379 cultivated overnight in a CO_2 incubator in Dulbecco's Modified Eagle Medium (DMEM;
380 Sigma-Aldrich) containing 10% fetal bovine serum (FBS), 50 U/mL penicillin, 50 μg/mL
381 streptomycin, and 10 ng/mL granulocyte-macrophage colony stimulating factor (GM-CSF) (R&D
382 Systems; 415-ML). The non-attached or weakly attached cells were collected and transferred to new
383 dishes and cultivated for an additional 5 days, then the cells were prepared for coculture experiments.
384 ***Coculture of cardiac fibroblasts and BMDMs in a Boyden chamber.*** Cardiac fibroblasts (2×10^4)
385 were plated on a 0.1% gelatin-coated 6-well dish (Thermo Scientific) and cultured for 48 hours in
386 DMEM containing 10% FBS, 50 U/mL penicillin, and 50 μg/ mL streptomycin. Cardiac fibroblasts
387 were damaged by 1 hour of coculture with 100 μM hydrogen peroxide (Sigma), as previously
388 described (45), with some modifications. Then, the damaged fibroblasts were maintained in DMEM
389 containing 10% FBS, 50 U/mL penicillin, and 50 μg/mL streptomycin. 2×10^4 BMDMs were seeded
390 onto polycarbonate membrane inserts (pore size, 0.4 μm; Thermo Scientific), which were set into the
391 wells containing fibroblasts. ErbB4 antibody (10 μg/mL; Thermo Scientific; catalog MA5-13016)
392 was added to the culture medium at the beginning of the coculture.
393 ***Induction of myocardial infarction (MI).*** MI was induced in mice by ligating the left coronary artery
394 under 2.0% isoflurane anesthesia and mechanical ventilation, as previously described (46). The
395 successful generation of MI was confirmed by changes in the color and motion of the left ventricular
396 walls. The survival rate and body weight change after MI were monitored daily.
397 ***Isolation of heart cells.*** Mouse heart cells were isolated as previously described (47). Immediately
398 after cervical dislocation, the aorta was clamped, and cooled Hank's balanced salt solution (HBSS;
399 Sigma-Aldrich) was injected into the left ventricular cavity. The isolated hearts were cut into 1-mm
400 pieces, digested with 0.05% collagenase II (Sigma-Aldrich) at 37 °C for 15 minutes and filtered with

401 a 40-μm cell strainer (BD Falcon). The remnant heart tissues were again digested with a fresh
402 digestion solution and filtered similarly; this cycle was repeated 5 times. The suspension obtained at
403 each cycle was combined and subjected to flow cytometric analyses or fluorescence-activated cell
404 sorting (FACS) after erythrocytes were depleted with Red Cell Lysis Buffer (BioLegend) according to
405 the manufacturer's protocol.

406 ***Flow cytometry and FACS.*** The isolated cells were resuspended in FACS buffer (HBSS plus 2 mM
407 EDTA plus 0.5% BSA) and preincubated with an anti-mouse CD16/CD32 Ab (rat, 1:100 dilution;
408 eBioscience; catalog 14-0161) to block the Fc receptor. The dead cells and debris were excluded by
409 forward scatter/side scatter (FSC/SSC) and DAPI staining (1:1,000 dilution; Sigma-Aldrich). To
410 determine their phenotypes, the cells were stained with the following Abs for 3 hours at 4 °C:
411 APC-conjugated anti-CD11b Ab (rat, 1:100 dilution; eBioscience; catalog 17-0112); phycoerythrin-
412 (PE-)conjugated anti-F4/80 Ab (rat, 1:20 dilution; eBioscience; catalog 12-4801); and Alexa Fluor
413 488-conjugated anti-CD206 Ab (rat, 1:50 dilution; BioLegend; catalog 141709). Cell sorting was
414 performed with a FACSAria II (BD Biosciences).

415 ***Isolation of cardiac fibroblasts.*** Cardiac fibroblasts were isolated from Wistar rats (Charles River
416 Laboratories), as previously described (48), with some modifications. The isolated rat heart was cut
417 into 1-mm pieces, and the fragments were plated evenly in 10-cm 0.1% gelatin-coated dishes so that
418 they did not touch each other. Each fragment was covered by a droplet of DMEM medium containing
419 10% FBS, 50 U/ mL penicillin, and 50 μg/mL streptomycin and incubated for 24 hours at 37 °C in a
420 CO_2 incubator. Then, sufficient medium was added to cover the entire bottom of the culture dish, and
421 the culture was incubated for an additional 24 hours. After this period, sufficient medium was added
422 to completely cover the heart fragments, and the culture was continued for an additional 5 days. When
423 fibroblast outgrowth was observed, the cells were collected by trypsinization. The fibroblasts were
424 maintained in DMEM containing 10% FBS, 50 U/mL penicillin, and 50 μg/mL streptomycin in 0.1%
425 gelatin-coated culture flasks. The cells were used at passage 3 or 4.

426 ***RNA extraction and real-time polymerase chain reaction (PCR).*** Total RNA was extracted from
427 cells or the heart tissue with the Gene Jet PCR purification Kit (Thermo Scientific) and quantified
428 with a Nano-Drop 8000 spectrophotometer (Thermo Scientific). cDNA was synthesized with the

429 high-capacity cDNA Reverse Transcription Kit (Applied Biosystems) from 25 ng and 150 ng of total
430 RNAs from M2-macrophages and the heart tissues, respectively. Real-time PCR was performed by a
431 QuantStudio (Applied Biosystems) with a SYBR PremixExTaqII (Takara Bio) in the following
432 conditions: 95 °C for 30 seconds followed by 40 cycles at 95 °C for 5 seconds and 60 °C for 30
433 seconds. Gene expression levels were normalized by *Gapdh*. The primers used are shown in the
434 Supplemental Table 1.
435 ***Microarray analysis.*** Total RNA of $CD206^{+}F4/80^{+}CD11b^{+}$ M2-like macrophages were isolated by
436 FACS (see above) from the heart and peritoneal cavity, amplified with the RNA Amplification
437 System (NuGEN) and subjected to an Illumina's beads array platform with a Mouse WG-6 v2.0
438 Expression BeadChip (Illumina). Two independent biological replicates were prepared for each group
439 category. The median per chip normalization was performed in each array. We analyzed only genes
440 whose signal intensity was above the value of 90 in one of the biological duplicates. A 2-fold change
441 cut-off was used to identify differential lay expressed genes.
442 ***Immunohistochemistry.*** Immediately after cervical dislocation, the aorta of the mouse was clamped
443 and ice-cold PBS was injected into the left ventricular cavity. The mouse heart was then perfused with
444 ice-cold 4% paraformaldehyde in PBS. The heart was removed, cut and embedded in optimal cutting
445 temperature (OCT) compound (VWR International) and frozen in isopentane chilled in liquid nitrogen.
446 The frozen tissue sections (8-µm thick) were prepared, and the non-specific antibody-binding sites
447 were pre-blocked with the blocking buffer (PBS plus 5% of goat serum). Then, the primary antibodies
448 were applied overnight at 4 °C. After rinsing 3 times for 15 minutes in PBS, the sections were next
449 incubated with appropriate fluorophore-conjugated secondary antibodies and
450 4',6-diamidino-2-phenylindole (DAPI) (Sigma-Aldrich, D9542) in the blocking buffer for 1 hour at
451 room temperature. Stained sections were mounted with a DAKO Fluorescence Mounting Medium
452 (Agilent, S302380-2). The primary and secondary antibodies used in this study are shown in the
453 Supplemental Table 2.
454 ***Picrosirius red staining.*** The 8-µm thick frozen sections were incubated in 1.5% phosphomolybdic
455 acid for 60 minutes, then in 0.1% Picrosirius Red for 15 minutes, and finally in 0.5% acetic acid
456 solution for 3 minutes. After dehydration by adding increasing concentrations of ethanol to xylene,

457 the sections were mounted with the DPX mounting medium (VWR International). The infarct area
458 was defined as the area in which more than 90% of cardiomyocytes were lost.
459 ***Masson trichrome staining.*** The frozen tissue sections (8 μm thick) were prepared as above and
460 stained with the Trichrome Stain Kit (Scy Tek Laboratories) according to the manufacturer's
461 instructions.
462 ***Immunocytochemistry.*** The cells were fixed by 4% of paraformaldehyde in PBS for 5 minutes at
463 room temperature. Apart from the cells to be used for surface antigen staining, cells were incubated in
464 PBS containing 0.1% of Triton x100 for 5 minutes at room temperature. Non-specific antibody
465 binding sites were pre-blocked with PBS containing 5% of goat serum for 30 minutes at the room
466 temperature. Then, primary antibodies were applied to the cells for 1 hour at room temperature. The
467 primary antibodies used were as follows: anti-vimentin (1:100, Abcam, ab24525), anti-cleaved
468 caspase-3 (1:100, Cell Signaling, 9661), anti-Ki-67 (1:100, eBioscience, 14-5698), and anti-αSMA
469 (1:00, Abcam, ab5694). After rinsing, cells were incubated with the fluorophore-conjugated
470 secondary antibodies (1:300, AlexaFluor 488-conjugated or AlexaFluor 594-conjugated polyclonal,
471 Invitrogen) and DAPI in blocking buffer for 1 hour at room temperature.
472 ***Imaging and analysis.*** All digital images were acquired with an All-in-One microscope (BZ-8000;
473 KEYENCE). All image analyses were performed by importing images as TIFF files into National
474 Institute of Health image-analysis software (ImageJ software). For quantification of fibrin formation,
475 the fibrin area was quantified as the percentage of the fibrin positive area on the whole screen.
476 Images were acquired at 5 independent regions and analyzed. A color threshold function of ImageJ
477 was applied to measure macrophages, fibroblasts, fibrin clot area, and cell size of cultured fibroblasts.
478 ***Immunoblotting.*** For western blot analysis, tissue was frozen and crushed; then, it was lysed by
479 T-PER Tissue Protein Extraction Regent (Thermo Scientific, 78510), according to the
480 manufacturer's protocol. Protein concentration was measured with a Nano-Drop 8000
481 spectrophotometer (Thermo Scientific), and 50-μg protein lysates were separated by PAGE,
482 transferred onto a polyvinylidene difluoride membrane and then identified by immunoblotting by
483 using the primary and second antibodies shown in the Supplemental Table 3. The protein bands

484 were visualized with a Super Signal West Pico Substrate (Thermo Scientific, 34077), according to
485 the manufacturer's instructions.
486 ***Statistics.*** All statistical tests were performed with GraphPad Prism software, version 8 (GraphPad
487 Software). Data represent the mean ± SEM. For comparisons between multiple groups,
488 repeated-measures analysis of variance (ANOVA) or 1- or 2-way ANOVA was performed, followed
489 by Bonferroni's post hoc test. Two groups were compared with the 2-tailed, unpaired Student's *t* test.
490 Cardiac rupture rates were compared with the χ^2test, and survival curves were compared with the
491 log-rank test.
492
493 **Author contributions**
494
495 MS and KS conceived and designed the study. MS conducted most of the experiments and
496 acquired the data, with professional support from AY and KS. All authors participated in the analysis
497 and interpretation of the data. MS and KS primarily wrote and edited the manuscript, with input from
498 all other authors.
499
500 **Acknowledgments**
501
502 This project was funded by the Uehara Memorial Foundation, the SENSHIN Medical Research
503 Foundation, a Grant-in-Aid for Scientific Research (C), the Mochida Memorial Foundation for
504 Medical and Pharmaceutical Research, the Takeda Science Foundation, and the Public Trust Surgery
505 Research Fund. We thank Ellen Knapp, PhD, from Edanz Group
506 (https://en-author-services.edanz.com/ac) for editing a draft of this manuscript.
507

508 **References**

509 1. Zhu F, Li Y, Zhang J, Piao C, Liu T, Li HH, et al. Senescent cardiac fibroblast is
510 critical for cardiac fibrosis after myocardial infarction. *PLoS One.* 2013;8(9):e74535.
511 2. Dickstein K, Cohen-Solal A, Filippatos G, McMurray JJ, Ponikowski P,
512 Poole-Wilson PA, et al. ESC Guidelines for the diagnosis and treatment of acute and
513 chronic heart failure 2008: the Task Force for the Diagnosis and Treatment of Acute
514 and Chronic Heart Failure 2008 of the European Society of Cardiology. Developed in
515 collaboration with the Heart Failure Association of the ESC (HFA) and endorsed by
516 the European Society of Intensive Care Medicine (ESICM). *Eur Heart J.*
517 2008;29(19):2388-442.
518 3. Gemberling M, Karra R, Dickson AL, and Poss KD. Nrg1 is an injury-induced
519 cardiomyocyte mitogen for the endogenous heart regeneration program in zebrafish.
520 *Elife.* 2015;4.
521 4. Gould KE, Taffet GE, Michael LH, Christie RM, Konkol DL, Pocius JS, et al. Heart
522 failure and greater infarct expansion in middle-aged mice: a relevant model for
523 postinfarction failure. *Am J Physiol Heart Circ Physiol.* 2002;282(2):H615-21.
524 5. Takemura G, Ohno M, Hayakawa Y, Misao J, Kanoh M, Ohno A, et al. Role of
525 apoptosis in the disappearance of infiltrated and proliferated interstitial cells after
526 myocardial infarction. *Circ Res.* 1998;82(11):1130-8.
527 6. Sharpless NE, and Sherr CJ. Forging a signature of in vivo senescence. *Nat Rev*
528 *Cancer.* 2015;15(7):397-408.
529 7. Munoz-Espin D, and Serrano M. Cellular senescence: from physiology to pathology.
530 *Nat Rev Mol Cell Biol.* 2014;15(7):482-96.

531 8. Coppe JP, Desprez PY, Krtolica A, and Campisi J. The senescence-associated
532 secretory phenotype: the dark side of tumor suppression. *Annu Rev Pathol.*
533 2010;5:99-118.
534 9. Alam P, Haile B, Arif M, Pandey R, Rokvic M, Nieman M, et al. Inhibition of
535 Senescence-Associated Genes Rb1 and Meis2 in Adult Cardiomyocytes Results in
536 Cell Cycle Reentry and Cardiac Repair Post-Myocardial Infarction. *J Am Heart Assoc.*
537 2019;8(15):e012089.
538 10. Hayakawa K, Takemura G, Kanoh M, Li Y, Koda M, Kawase Y, et al. Inhibition of
539 granulation tissue cell apoptosis during the subacute stage of myocardial infarction
540 improves cardiac remodeling and dysfunction at the chronic stage. *Circulation.*
541 2003;108(1):104-9.
542 11. Childs BG, Li H, and van Deursen JM. Senescent cells: a therapeutic target for
543 cardiovascular disease. *J Clin Invest.* 2018;128(4):1217-28.
544 12. Aurora AB, Porrello ER, Tan W, Mahmoud AI, Hill JA, Bassel-Duby R, et al.
545 Macrophages are required for neonatal heart regeneration. *J Clin Invest.*
546 2014;124(3):1382-92.
547 13. Shiraishi M, Shintani Y, Shintani Y, Ishida H, Saba R, Yamaguchi A, et al.
548 Alternatively activated macrophages determine repair of the infarcted adult murine
549 heart. *J Clin Invest.* 2016;126(6):2151-66.
550 14. Meyer D, Yamaai T, Garratt A, Riethmacher-Sonnenberg E, Kane D, Theill LE, et al.
551 Isoform-specific expression and function of neuregulin. *Development.*
552 1997;124(18):3575-86.
553 15. Fuller SJ, Sivarajah K, and Sugden PH. ErbB receptors, their ligands, and the
554 consequences of their activation and inhibition in the myocardium. *J Mol Cell Cardiol.*
555 2008;44(5):831-54.

556 16. Bersell K, Arab S, Haring B, and Kuhn B. Neuregulin1/ErbB4 signaling induces
557 cardiomyocyte proliferation and repair of heart injury. *Cell.* 2009;138(2):257-70.
558 17. Hedhli N, Huang Q, Kalinowski A, Palmeri M, Hu X, Russell RR, et al.
559 Endothelium-derived neuregulin protects the heart against ischemic injury.
560 *Circulation.* 2011;123(20):2254-62.
561 18. Polizzotti BD, Ganapathy B, Walsh S, Choudhury S, Ammanamanchi N, Bennett DG,
562 et al. Neuregulin stimulation of cardiomyocyte regeneration in mice and human
563 myocardium reveals a therapeutic window. *Sci Transl Med.* 2015;7(281):281ra45.
564 19. Yutzey KE. Regenerative biology: Neuregulin 1 makes heart muscle. *Nature.*
565 2015;520(7548):445-6.
566 20. Lemmens K, Doggen K, and De Keulenaer GW. Role of neuregulin-1/ErbB signaling
567 in cardiovascular physiology and disease: implications for therapy of heart failure.
568 *Circulation.* 2007;116(8):954-60.
569 21. Krizhanovsky V, Yon M, Dickins RA, Hearn S, Simon J, Miething C, et al.
570 Senescence of activated stellate cells limits liver fibrosis. *Cell.* 2008;134(4):657-67.
571 22. van Deursen JM. The role of senescent cells in ageing. *Nature.*
572 2014;509(7501):439-46.
573 23. Olayioye MA, Neve RM, Lane HA, and Hynes NE. The ErbB signaling network:
574 receptor heterodimerization in development and cancer. *EMBO J.*
575 2000;19(13):3159-67.
576 24. Uray IP, Connelly JH, Thomazy V, Shipley GL, Vaughn WK, Frazier OH, et al. Left
577 ventricular unloading alters receptor tyrosine kinase expression in the failing human
578 heart. *J Heart Lung Transplant.* 2002;21(7):771-82.
579 25. Suzuki T, Arumugam P, Sakagami T, Lachmann N, Chalk C, Sallese A, et al.
580 Pulmonary macrophage transplantation therapy. *Nature.* 2014;514(7523):450-4.

581 26. van den Borne SW, Diez J, Blankesteijn WM, Verjans J, Hofstra L, and Narula J.
582 Myocardial remodeling after infarction: the role of myofibroblasts. *Nat Rev Cardiol.*
583 2010;7(1):30-7.
584 27. Shinde AV, and Frangogiannis NG. Fibroblasts in myocardial infarction: a role in
585 inflammation and repair. *J Mol Cell Cardiol.* 2014;70:74-82.
586 28. Park S, Jiang Z, Mortenson ED, Deng L, Radkevich-Brown O, Yang X, et al. The
587 therapeutic effect of anti-HER2/neu antibody depends on both innate and adaptive
588 immunity. *Cancer Cell.* 2010;18(2):160-70.
589 29. ElZarrad MK, Mukhopadhyay P, Mohan N, Hao E, Dokmanovic M, Hirsch DS, et al.
590 Trastuzumab alters the expression of genes essential for cardiac function and induces
591 ultrastructural changes of cardiomyocytes in mice. *PLoS One.* 2013;8(11):e79543.
592 30. Sasaki M, Miyakoshi M, Sato Y, and Nakanuma Y. Modulation of the
593 microenvironment by senescent biliary epithelial cells may be involved in the
594 pathogenesis of primary biliary cirrhosis. *J Hepatol.* 2010;53(2):318-25.
595 31. Kuramochi Y, Cote GM, Guo X, Lebrasseur NK, Cui L, Liao R, et al. Cardiac
596 endothelial cells regulate reactive oxygen species-induced cardiomyocyte apoptosis
597 through neuregulin-1beta/erbB4 signaling. *J Biol Chem.* 2004;279(49):51141-7.
598 32. Baliga RR, Pimental DR, Zhao YY, Simmons WW, Marchionni MA, Sawyer DB, et
599 al. NRG-1-induced cardiomyocyte hypertrophy. Role of PI-3-kinase, p70(S6K), and
600 MEK-MAPK-RSK. *Am J Physiol.* 1999;277(5 Pt 2):H2026-37.
601 33. Gelb BD, and Tartaglia M. RAS signaling pathway mutations and hypertrophic
602 cardiomyopathy: getting into and out of the thick of it. *J Clin Invest.*
603 2011;121(3):844-7.

604 34. Long X, Boluyt MO, Hipolito ML, Lundberg MS, Zheng JS, O'Neill L, et al. p53 and
605 the hypoxia-induced apoptosis of cultured neonatal rat cardiac myocytes. *J Clin Invest.*
606 1997;99(11):2635-43.
607 35. Polyak K, Xia Y, Zweier JL, Kinzler KW, and Vogelstein B. A model for
608 p53-induced apoptosis. *Nature.* 1997;389(6648):300-5.
609 36. Deng C, Zhang P, Harper JW, Elledge SJ, and Leder P. Mice lacking p21CIP1/WAF1
610 undergo normal development, but are defective in G1 checkpoint control. *Cell.*
611 1995;82(4):675-84.
612 37. Wang YA, Elson A, and Leder P. Loss of p21 increases sensitivity to ionizing
613 radiation and delays the onset of lymphoma in atm-deficient mice. *Proc Natl Acad Sci*
614 *U S A.* 1997;94(26):14590-5.
615 38. Childs BG, Durik M, Baker DJ, and van Deursen JM. Cellular senescence in aging
616 and age-related disease: from mechanisms to therapy. *Nat Med.* 2015;21(12):1424-35.
617 39. Alcorta DA, Xiong Y, Phelps D, Hannon G, Beach D, and Barrett JC. Involvement of
618 the cyclin-dependent kinase inhibitor p16 (INK4a) in replicative senescence of
619 normal human fibroblasts. *Proc Natl Acad Sci U S A.* 1996;93(24):13742-7.
620 40. Stein GH, Drullinger LF, Soulard A, and Dulic V. Differential roles for
621 cyclin-dependent kinase inhibitors p21 and p16 in the mechanisms of senescence and
622 differentiation in human fibroblasts. *Mol Cell Biol.* 1999;19(3):2109-17.
623 41. Serrano M, Lin AW, McCurrach ME, Beach D, and Lowe SW. Oncogenic ras
624 provokes premature cell senescence associated with accumulation of p53 and
625 p16INK4a. *Cell.* 1997;88(5):593-602.
626 42. Ikeda N, Asano K, Kikuchi K, Uchida Y, Ikegami H, Takagi R, et al. Emergence of
627 immunoregulatory Ym1(+)Ly6C(hi) monocytes during recovery phase of tissue
628 injury. *Sci Immunol.* 2018;3(28).

629 43. Acosta JC, Banito A, Wuestefeld T, Georgilis A, Janich P, Morton JP, et al. A
630 complex secretory program orchestrated by the inflammasome controls paracrine
631 senescence. *Nat Cell Biol.* 2013;15(8):978-90.
632 44. Yu JS, and Cui W. Proliferation, survival and metabolism: the role of
633 PI3K/AKT/mTOR signalling in pluripotency and cell fate determination.
634 *Development.* 2016;143(17):3050-60.
635 45. Bladier C, Wolvetang EJ, Hutchinson P, de Haan JB, and Kola I. Response of a
636 primary human fibroblast cell line to H2O2: senescence-like growth arrest or
637 apoptosis? *Cell Growth Differ.* 1997;8(5):589-98.
638 46. Tano N, Narita T, Kaneko M, Ikebe C, Coppen SR, Campbell NG, et al. Epicardial
639 placement of mesenchymal stromal cell-sheets for the treatment of ischemic
640 cardiomyopathy; in vivo proof-of-concept study. *Mol Ther.* 2014;22(10):1864-71.
641 47. Shintani Y, Kapoor A, Kaneko M, Smolenski RT, D'Acquisto F, Coppen SR, et al.
642 TLR9 mediates cellular protection by modulating energy metabolism in
643 cardiomyocytes and neurons. *Proc Natl Acad Sci U S A.* 2013;110(13):5109-14.
644 48. Leicht M, Greipel N, and Zimmer H. Comitogenic effect of catecholamines on rat
645 cardiac fibroblasts in culture. *Cardiovasc Res.* 2000;48(2):274-84.
646

Figure 1.

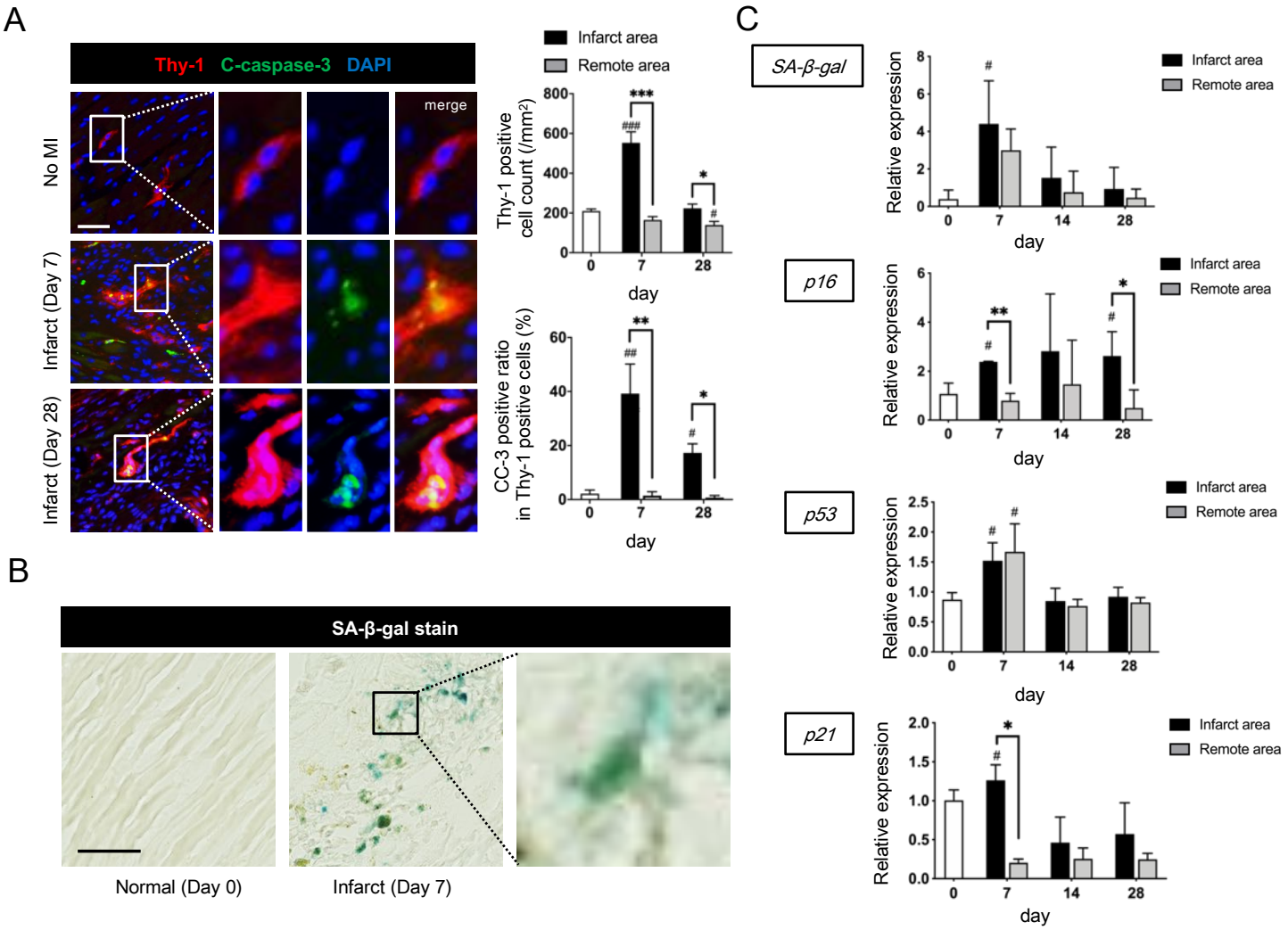

Figure 1. ***Cardiac fibroblasts underwent apoptosis and senescence after MI.***

(A) Double immunofluorescence staining for Thy1 and cleaved caspase 3 (CC-3) demonstrated that apoptosis of cardiac fibroblasts in the infarct area was exacerbated at post-myocardial infarction (MI) days 7 and 28 compared with the remote area. Scale bars: 100 μm. $n = 4$ in each group.

(B) SA-β-Gal staining demonstrated that spindle-shaped senescent fibroblasts accumulated in the infarct area. Scale bars: 100 μm.

(C) Quantitative reverse transcription polymerase chain reaction analysis showed the post-MI upregulation of senescence-associated genes in the infarct area at post-MI day 7 compared with the no-MI heart (day 0). $n = 4$ in each group. Data represent the mean ± SEM. $^{*}P < 0.05$, $^{**}P < 0.01$, $^{***}P < 0.005$ versus the remote area; $^{\#}P < 0.05$, $^{\#\#}P < 0.01$, $^{\#\#\#}P < 0.005$ versus the no-MI heart; 1-way ANOVA.

Figure 2.

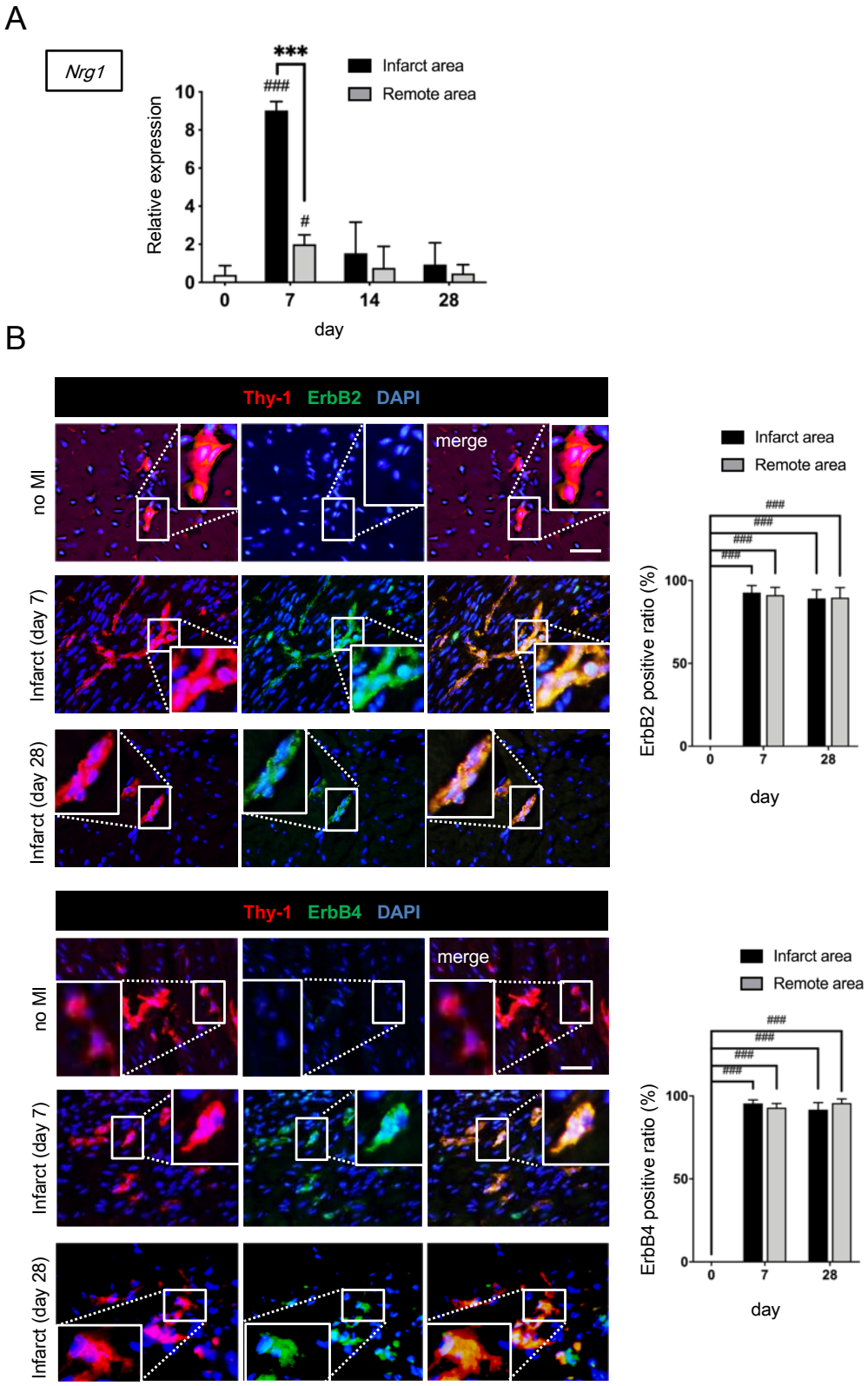

Figure 2. ***Nrg1 was upregulated in the infarct myocardium, while cardiac fibroblasts expressed Nrg1 receptors.***
(A) qRT-PCR analysis confirmed the post-MI upregulation of *Nrg1*. Expression levels relative to that of intact heart are presented. $n = 4$ in each group.

(B) Immunohistochemistry demonstrated that the ratio of ErbB4$^+$ fibroblasts (percentage of Thy1$^+$ErbB4$^+$ myofibroblasts/percentage of Thy1$^+$ fibroblasts) was markedly increased in the post-MI heart. Scale bars: 100 μm. $n = 4$ in each group. Data represent the mean ± SEM. $^*P < 0.05$, $^{**}P < 0.01$, $^{***}P < 0.005$ versus the remote area; $^{\#}P < 0.05$, $^{\#\#}P < 0.01$, $^{\#\#\#}P < 0.005$ versus the no-MI heart; 1-way ANOVA.

Figure 3.

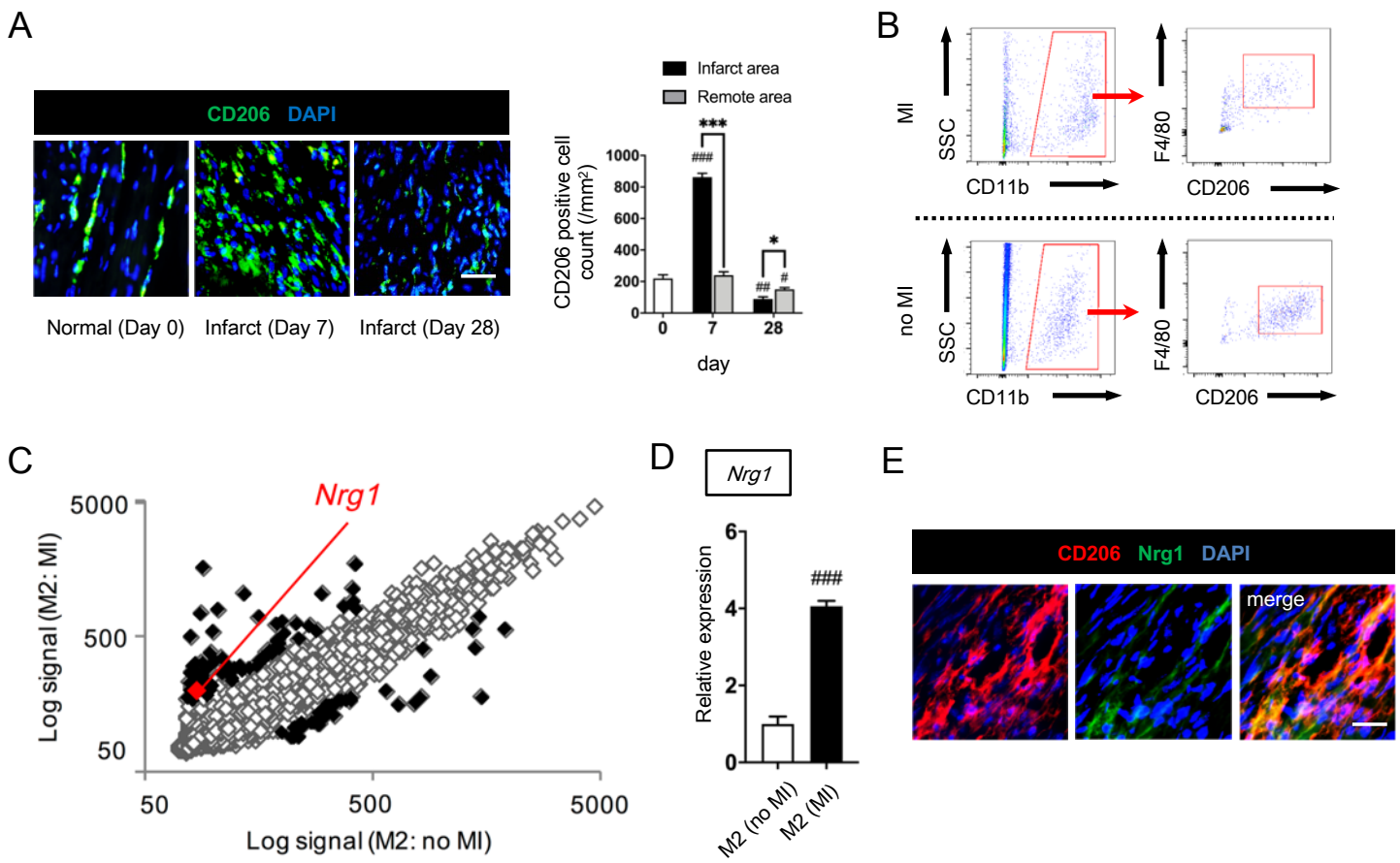

Figure 3. ***M2-like macrophages accumulated in the infarct and expressed Nrg1.***

(A) Immunohistochemistry showed that the accumulation of CD206$^+$ M2-like macrophages was increased in the infarct area, with a post-myocardial infarction (MI) peak on day 7. Scale bars: 100 μm. $n = 4$ in each group. Data represent the mean ± SEM. $^*P < 0.05$, $^{**}P < 0.01$, $^{***}P < 0.005$ versus the remote area; $^{\#}P < 0.05$, $^{\#\#}P < 0.01$, $^{\#\#\#}P < 0.005$ versus the no-MI heart; 1-way ANOVA.

(B) Flow cytometric analysis confirmed that CD206$^+$F4/80$^+$CD11b$^+$ M2-like macrophages were present in normal, no-myocardial infarction (no-MI) hearts and in day 7 post-MI hearts of adult C57BL/6 mice. $n = 6$ in each group.

(C) Microarray analysis demonstrated that M2 after myocardial infarction (M2: MI) had a different expression profile from that of M2: no MI. Scatter plot revealed that 70 genes were upregulated and 39 were downregulated in M2: MI macrophages compared with M2: no MI macrophages. The upregulated genes included neuregulin 1 (*Nrg1*).

(D) Quantitative reverse transcription polymerase chain reaction analysis confirmed the post-MI upregulation of *Nrg1* in CD206$^+$F4/80$^+$CD11b$^+$ cardiac M2-like macrophages [M2: MI]. $n = 4$ in each group. Data represent the mean ± SEM. $^{\#}P < 0.05$, $^{\#\#}P < 0.01$, $^{\#\#\#}P < 0.005$ versus M2: no MI; 2-tailed, unpaired Student's *t* test.

(E) Double immunofluorescence staining for CD206$^+$ M2-like macrophages and neuregulin 1 (Nrg1) demonstrated Nrg1 expression on the surface of CD206$^+$ M2-like macrophages . Scale bars: 100 μm. $n = 4$ in each group.

Figure 4.

A

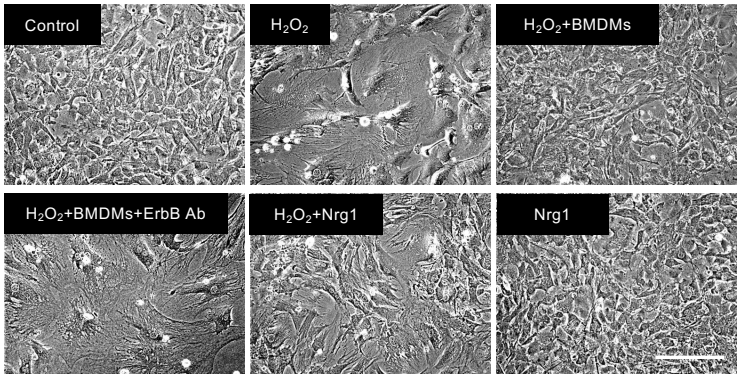

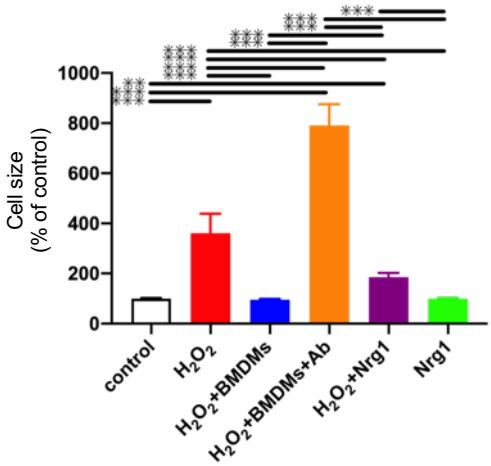

B

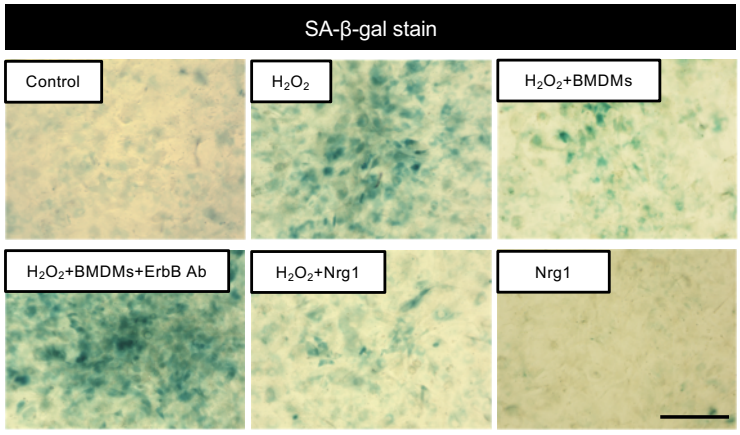

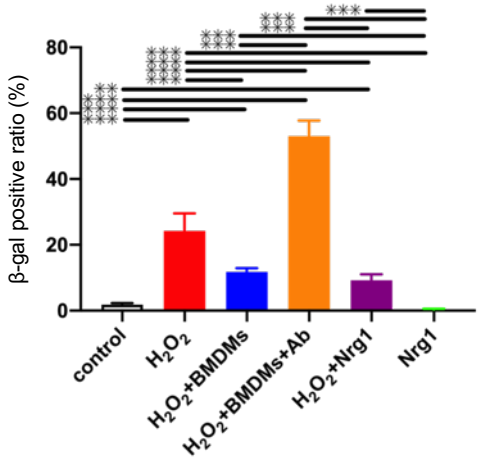

C

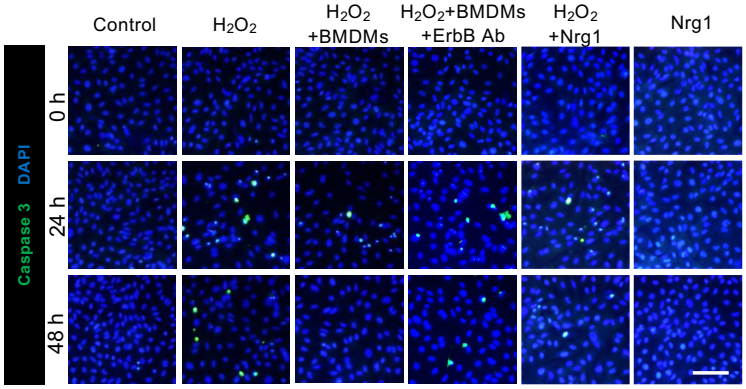

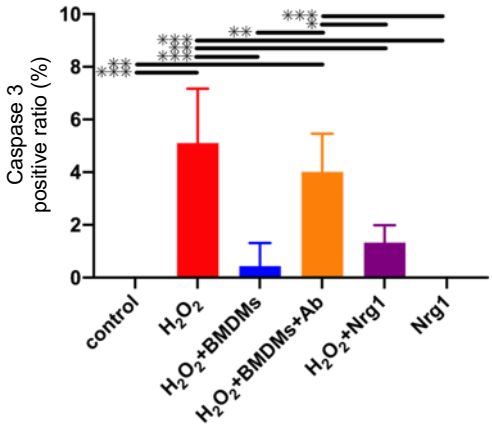

D

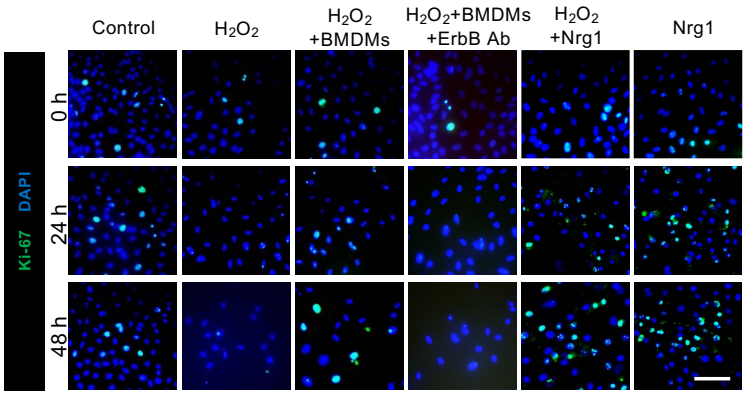

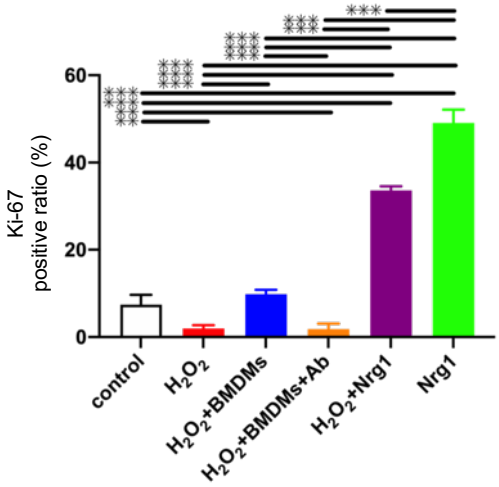

Figure 4. ***Bone marrow-derived macrophages attenuated H_2O_2-induced apoptosis and senescence of cardiac fibroblasts via Nrg1 secretion.***

(A) Representative images from phase-contrast microscopy. Treatment with hydrogen peroxide solution (H_2O_2) changed the spindle-shaped appearance to significantly enlarged, flattened morphology. After addition of bone marrow-derived macrophages (BMDMs), fibroblasts returned to spindle-shaped morphology. After addition of ErbB antibody (Ab), fibroblasts displayed the same gross morphology as senescent fibroblasts treated with H_2O_2. Recombinant neuregulin 1 (Nrg1) similarly changed the gross morphology to spindle-shaped. Scale bars: 100 μm. $n = 4$ in each group.

(B) SA-β-Gal staining showed that senescence of fibroblasts was exacerbated in coculture with H_2O_2 but not with H_2O_2 and BMDMs. This suppression of senescence was attenuated by coculture with ErbB Ab. Nrg1 suppressed fibroblast senescence. Scale bars: 100 μm. $n = 4$ in each group

(C) Apoptosis of cardiac fibroblasts (ratio of cleaved caspase-3^+DAPI$^+$ fibroblasts to DAPI$^+$ fibroblasts) was increased in the cocultures with H_2O_2 but decreased in those with BMDMs. This decreased apoptosis was eliminated by ErbB Ab. Nrg1 suppressed apoptosis. Nuclei were counterstained with 4',6-diamidino-2-phenylindole (DAPI). $n = 4$ in each group. Scale bars: 100 μm.

(D) Proliferation of cardiac fibroblasts (ratio of Ki-67^+ and DAPI$^+$ fibroblasts to DAPI$^+$ fibroblasts) was decreased in the cocultures with H_2O_2 but increased in those with BMDMs. This increased proliferation was eliminated by ErbB Ab. Nrg1 accelerated proliferation. Nuclei were counterstained with DAPI. Scale bars: 50 μm. $n = 4$ in each group. Data represent the mean ± SEM. $^*P < 0.05$, $^{**}P < 0.01$, $^{***}P < 0.005$ versus each group; 1-way ANOVA.

Figure 5.

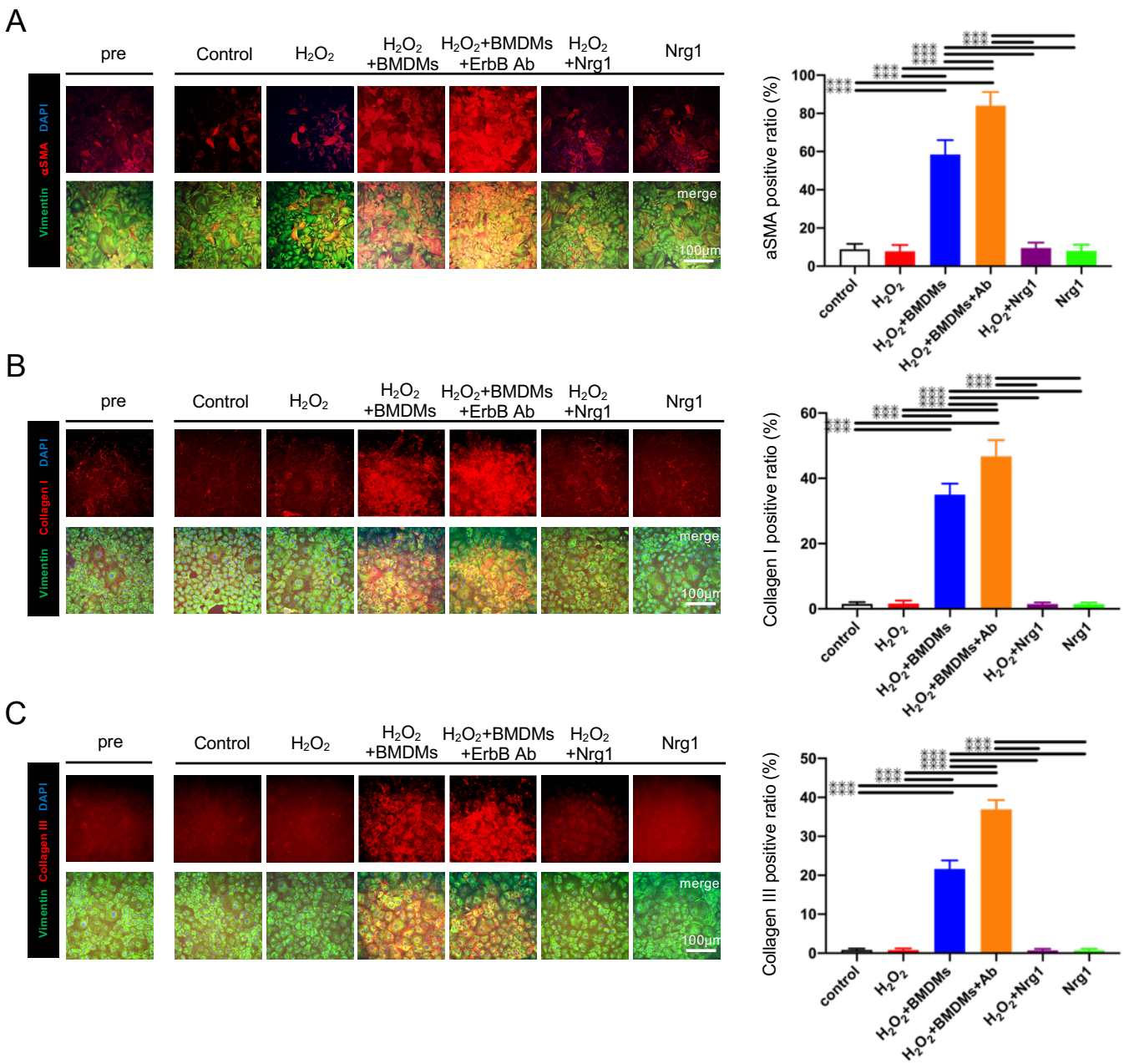

Figure 5. ***BMDMs promote fibroblast activation and collagen synthesis.***

(A-C) Representative images of immunocytochemical staining for (A) vimentin and αSMA, (B) vimentin and collagen I, and (C) vimentin and collagen III.

(A) Activation of cardiac fibroblasts (ratio of vimentin$^+$ and αSMA$^+$ myofibroblasts to vimentin$^+$ fibroblasts) was equable in the cocultures with hydrogen peroxide solution (H_2O_2) but markedly increased in those with bone marrow-derived macrophages (BMDMs). This increased activation was further accelerated by ErbB antibody (Ab). Addition of recombinant neuregulin 1 (Nrg1) did not affect activation of cardiac fibroblasts. Scale bars: 100 μm. $n = 4$ in each group.

(B) Collagen I synthesis was equable in the cocultures with H_2O_2 but significantly increased in those with BMDMs. This increased production was further enhanced by ErbB Ab. Addition of Nrg1 did not affect collagen I synthesis. Scale bars: 100 μm. $n = 4$ in each group.

(C) Collagen III synthesis exhibited a similar tendency as collagen I. Scale bars: 100 μm. $n = 4$ in each group. Data represent the mean ± SEM. $^*P < 0.05$, $^{**}P < 0.01$, $^{***}P < 0.005$ versus each group; 1-way ANOVA

Figure 6.

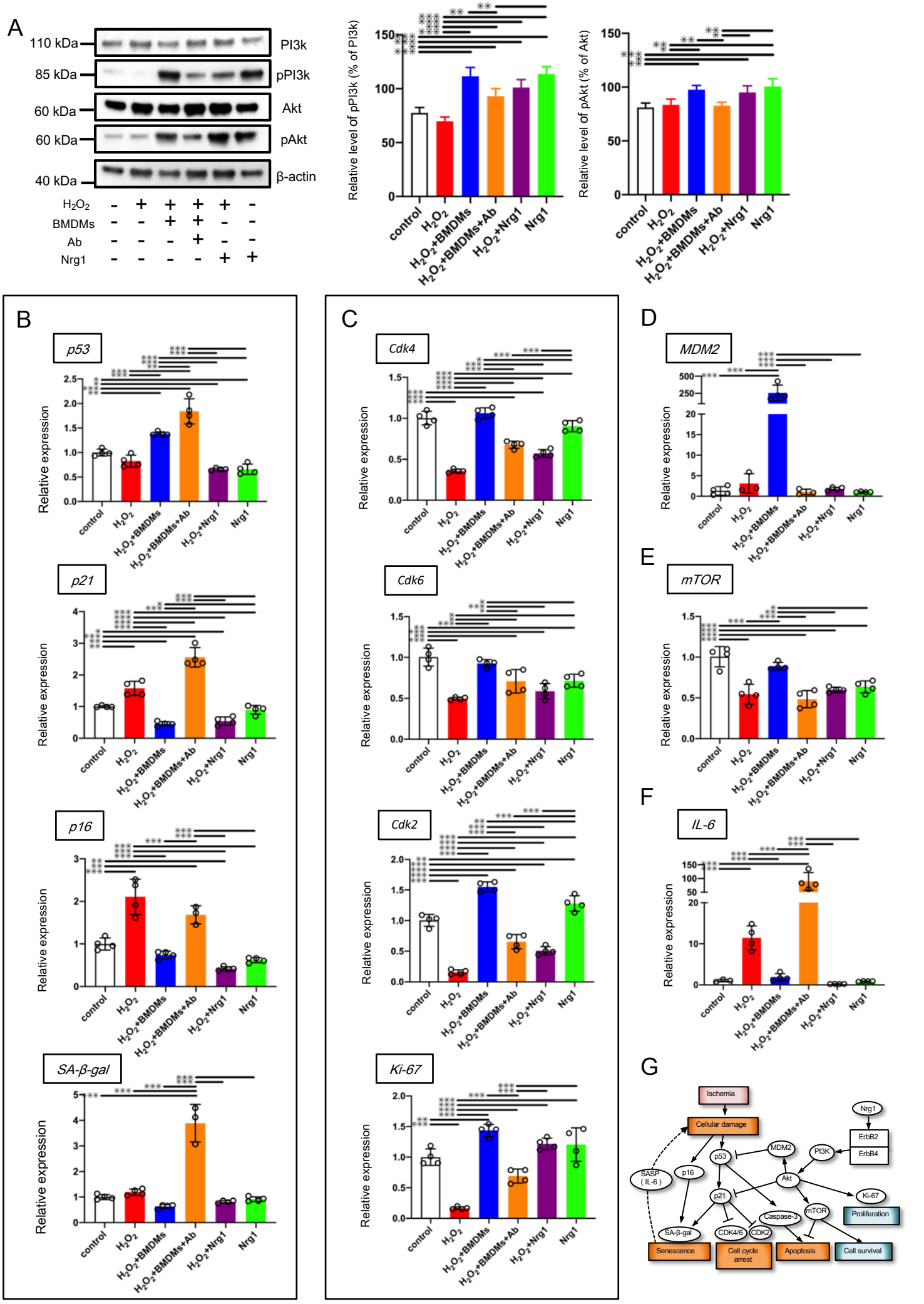
A
110 kDa
85 kDa
60 kDa
60 kDa
40 kDa
PI3k
pPI3k
Akt
pAkt
β-actin
H2O2
BMDMs
Ab
Nrg1
Relative level of pPI3k (% of PI3k)
Relative level of pAkt (% of Akt)
control
H2O2
H2O2+BMDMs
H2O2+BMDMs+Ab
H2O2+Nrg1
Nrg1
B
p53
p21
p16
SA-β-gal
C
Cdk4
Cdk6
Cdk2
Ki-67
D
MDM2
E
mTOR
F
IL-6
Relative expression
G
Ischemia
Cellular damage
Nrg1
ErbB2
ErbB4
PI3K
MDM2
p53
p16
SASP (IL-6)
Akt
p21
Ki-67
Proliferation
mTOR
Caspase-3
SA-β-gal
CDK4/6
CDK2
Senescence
Cell cycle arrest
Apoptosis
Cell survival

Figure 6. ***PI3K/Akt signaling pathway was associated with BMDM-attenuated apoptosis and senescence of cardiac fibroblasts through Nrg1.***

(A) Representative band of PI3K, pPI3K, Akt, pAkt, and β-actin. Bar graph showed that hydrogen peroxide solution (H_2O_2) alone did not affect activation of PI3K/AKT signaling in fibroblasts. Addition of bone marrow-derived macrophages (BMDMs) significantly activated the signaling pathway, and addition of ErbB antibody (Ab) impaired the activation. adding recombinant neuregulin 1 (Nrg1) stimulated the signaling pathway again. $n = 4$ in each group.

(B) Quantitative reverse transcription polymerase chain reaction analysis of cardiac fibroblasts with or without H_2O_2 / BMDMs / ErbB Ab. The expression levels of senescence-associated genes (*p53, p21, p16*, and *SA-β-Gal*) were increased in the cocultures with H_2O_2 with a time lapse but decreased in the cocultures with BMDMs. Adding ErbB Ab increased these expressions, and adding Nrg1 suppressed them. $n = 4$ in each group.

(C) The expression levels of cell cycle-associated genes (*Cdk4, Cdk6, Cdk2*, and *Ki-67*) were suppressed in the cocultures with H_2O_2 but recovered in those with BMDMs. Adding ErbB Ab decreased these expressions, and adding Nrg1 recovered these expressions. $n = 4$ in each group.

(D) p53 suppressor gene (*MDM2*) was significantly increased in coculture with BMDMs. $n = 4$ in each group.

(E) The expression levels of cell survival-associated gene (*mTOR*) were suppressed in coculture with H_2O_2 but recovered in coculture with BMDMs. Adding ErbB Ab suppressed the expression again, and adding Nrg1 increased it again.

(F) Senescence-associated secretory phenotype-associated gene (*IL-6*) was significantly increased in coculture with BMDMs and after adding ErbB Ab. $n = 4$ in each group. Data represent the mean ± SEM. $^*P < 0.05$, $^{**}P < 0.01$, $^{***}P < 0.005$ versus each group; 1-way ANOVA.

(G) Schematic representation and overview of the Nrg1/PI3K/AKT pathway. Ischemia contributes to the development of cellular damage, leading to senescence, cell cycle arrest, and apoptosis. Nrg1 binding to coreceptor ErbB2/ErbB4 leads to activation of PI3K/AKT and inactivation of p53 and p21. Arrowheads indicate stimulation, whereas hammerheads represent inhibition.

Figure 7.

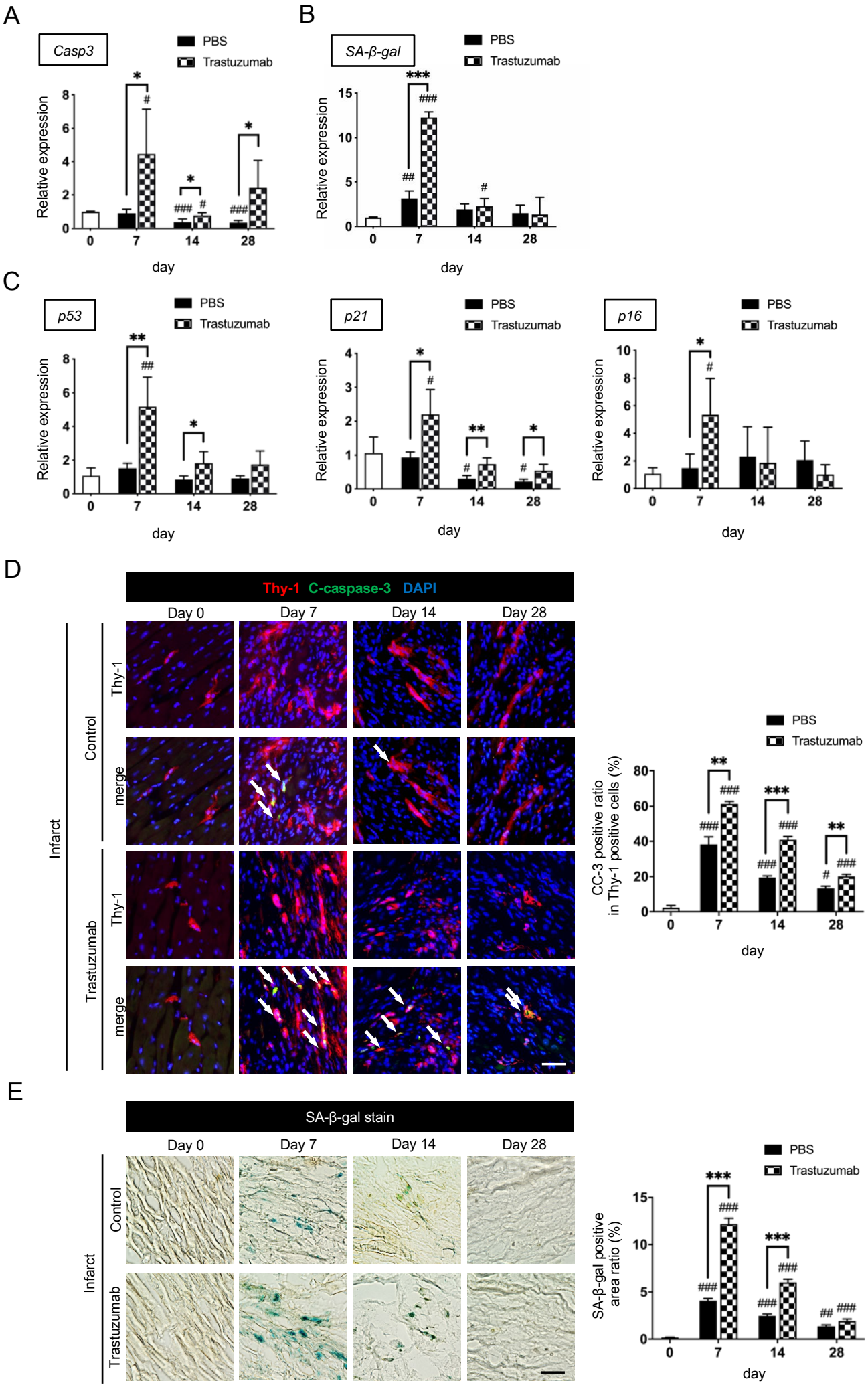
A
Casp3
PBS
Trastuzumab
Relative expression
day
B
SA-β-gal
C
p53
p21
p16
D
Thy-1 C-caspase-3 DAPI
Day 0
Day 7
Day 14
Day 28
Infarct
Control
Trastuzumab
Thy-1
merge
CC-3 positive ratio in Thy-1 positive cells (%)
E
SA-β-gal stain
SA-β-gal positive area ratio (%)

Figure 7. ***In vivo inhibition of Nrg1 signalling promotes apoptosis and senescence of cardiac fibroblasts.***

(A-C) Quantitative reverse transcription polymerase chain reaction analysis showed the post-myocardial infarction (MI) upregulation of (A) apoptosis-associated gene (*Casp3*), (B-C) senescence-associated genes (*SA-β-Gal, p53, p21*, and *p16* in mice after intraperitoneal trastuzumab injection compared with controls. n = 4 in each group.

(D) Double immunofluorescence staining for Thy1 and cleaved caspase 3 (CC-3) demonstrated that the ratio of apoptotic cardiac fibroblasts in the infarct area was increased in mice after intraperitoneal trastuzumab injection compared with controls at post-myocardial infarction (MI) days 7, 14 and 28. Arrow shows $Thy1^{+}CC\text{-}3^{+}$ cells. Scale bars: 100 μm. n = 4 in each group.

(E) SA-β-Gal staining demonstrated that senescence of cardiac cells in the infarct area was exacerbated in mice after intraperitoneal trastuzumab injection compared with controls at post-myocardial infarction (MI) days 7 and 14. Scale bars: 20 μm. n = 4 in each group. Data represent the mean ± SEM. $^{*}P < 0.05$, $^{**}P < 0.01$, $^{***}P < 0.005$ versus each group; $^{\#}P < 0.05$, $^{\#\#}P < 0.01$, $^{\#\#\#}P < 0.005$ versus the no-MI heart; 1-way ANOVA.

Figure 8.

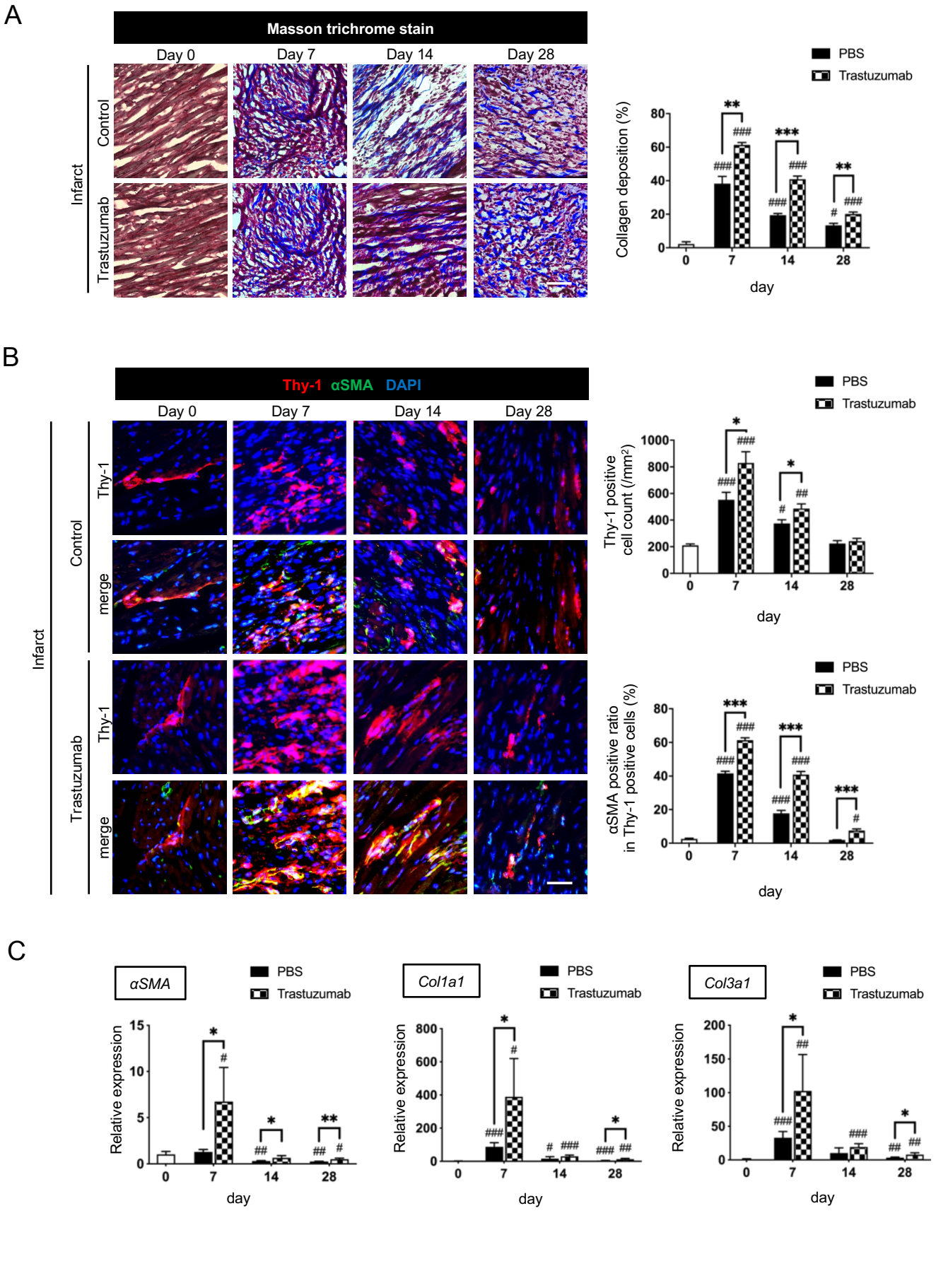
A
Masson trichrome stain
Day 0
Day 7
Day 14
Day 28
Infarct
Control
Trastuzumab
PBS
Trastuzumab
Collagen deposition (%)
day
B
Thy-1 αSMA DAPI
Thy-1
merge
Thy-1 positive cell count (/mm²)
αSMA positive ratio in Thy-1 positive cells (%)
C
αSMA
Col1a1
Col3a1
Relative expression

Figure 8. ***In vivo inhibition of Nrg1 signalling activates cardiac fibroblasts and exacerbates fibrosis.***

(A) Masson trichrome staining demonstrated that the deposition of collagen fibril was increased in the post-MI infarct area with a time lapse. Intraperitoneal trastuzumab injection significantly increased collagen fibril in the infarct area. Scale bars: 100 μm. $n = 4$ in each group.

(B) Double immunofluorescence staining for Thy1 and αSMA showed increased accumulation and activation of cardiac fibroblasts in the infarct area in the trastuzumab group compared with the control group. Scale bars: 100 μm. $n = 4$ in each group.

(C) Quantitative reverse transcription polymerase chain reaction (qRT-PCR) analysis showed the post-MI upregulation of fibrosis-associated genes (*αSMA, Col1a1,* and *Col3a1*) in mice after intraperitoneal trastuzumab injection mice compared with controls. $n = 4$ in each group. Data represent the mean ± SEM. $^{*}P < 0.05$, $^{**}P < 0.01$, $^{***}P < 0.005$ versus each group; $^{\#}P < 0.05$, $^{\#\#}P < 0.01$, $^{\#\#\#}P < 0.005$ versus the no-MI heart; 1-way ANOVA.

Figure 9.

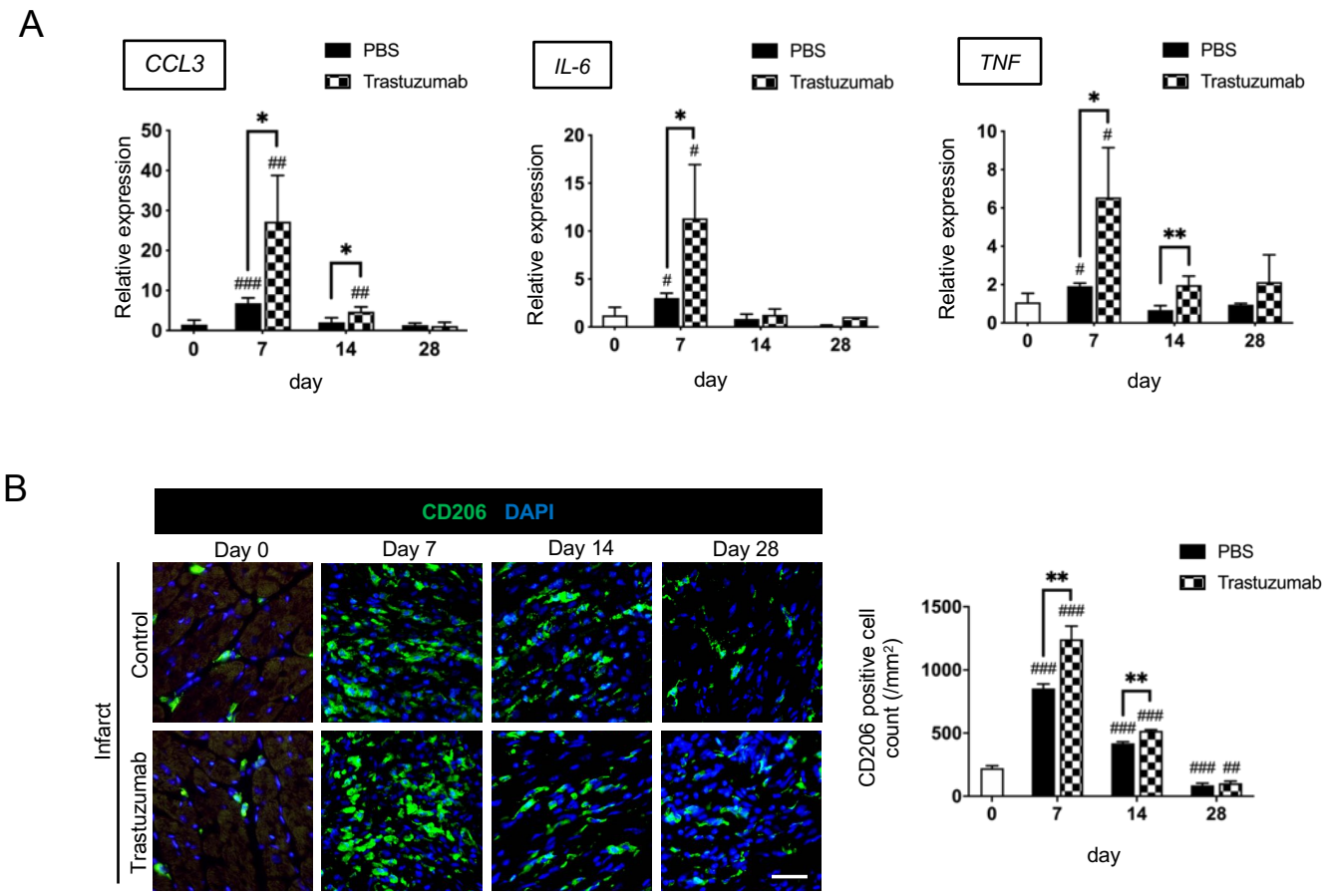

Figure 9. ***In vivo inhibition of Nrg1 signalling exacerbates myocardial inflammation and promotes accumulation of M2-like macrophages.***

(A) Quantitative reverse transcription polymerase chain reaction analysis showed the post-myocardial infarction (MI) upregulation of senescence-associated secretory phenotype-associated gene (CCl3, *IL-6* and *TNF*) in mice after intraperitoneal trastuzumab injection compared with controls. $n = 4$ in each group.

(B) Immunohistochemistry showed increased accumulation of CD206^{+} M2-like macrophages in the infarct area, with a post-myocardial infarction (MI) peak on day 7. Intraperitoneal trastuzumab injection significantly accelerated accumulation of CD206^{+} M2-like macrophages in the infarct area. Scale bars: 100 μm. $n = 4$ in each group. Data represent the mean ± SEM. $^{*}P < 0.05$, $^{**}P < 0.01$, $^{***}P < 0.005$ versus each group; $^{\#}P < 0.05$ $^{\#\#}P < 0.01$, $^{\#\#\#}P < 0.005$ versus the no-MI heart; 1-wayANOVA.

Figure 10.

A

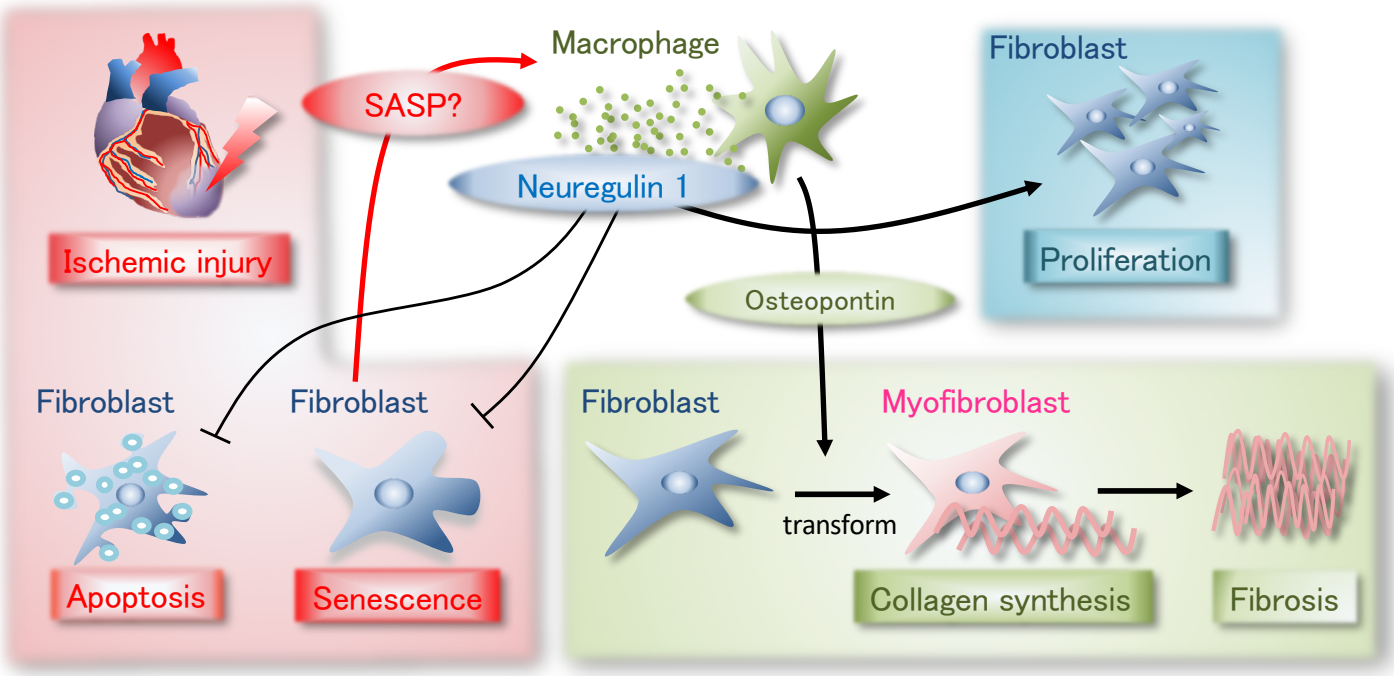

Figure 10. Schematic illustration of interrelationship between M2-like macrophages and cardiac fibroblasts.

Ischemic injury contributes to the development of cellular senescence and apoptosis. Senescent cells, including cardiac fibroblasts, show the senescence-associated secretory phenotype (SASP), resulting in activation of M2-like macrophages. M2-like macrophages suppress the senescence and apoptosis of fibroblasts and simultaneously accelerate proliferation. Osteopontin-mediated induction of fibroblasts into myofibroblasts promotes fibrosis (11).